Brine grades in Andean salars: When basin size matters A review of the Lithium Triangle

Romina Lucrecia López Steinmetz, Stefano Salvi

Brine grades in Andean salars: When basin size matters A review of the Lithium Triangle

Romina Lucrecia López Steinmetz, Stefano Salvi

PII: S0012-8252(21)00115-X

DOI: https://doi.org/10.1016/j.earscirev.2021.103615

Reference: EARTH 103615

To appear in: *Earth-Science Reviews*

Received date: 16 May 2020

Revised date: 9 February 2021

Accepted date: 27 March 2021

Please cite this article as: R.L.L. Steinmetz and S. Salvi, Brine grades in Andean salars: When basin size matters A review of the Lithium Triangle, *Earth-Science Reviews* (2021), https://doi.org/10.1016/j.earscirev.2021.103615

Brine grades in Andean salars: when basin size matters A review of the Lithium Triangle

Romina Lucrecia López Steinmetz[1,*] lucrecialopezsteinmetz@hotmail.com, Stefano Salvi[2] stefano.salvi@get.omp.eu

[1]IDEVEA (CONICET - UTN), Av. GRAL. J.J. Urquiza 314, 5600 San Rafael, Mendoza, Argentina

[2]University of Toulouse, CNRS, GET, IRD, OMP, 14 Av. Edouard Belin, Toulouse 31400, France

[*]Corresponding author

Abstract

The Lithium Triangle, a zone of the Central Andes characterized by the presence of lithium (Li)-rich salt pans within endorheic basins, has gained a worldwide reputation chiefly due to its exceptional Li brine-type deposits. We summarize scientific hydrochemical reports, totalizing a data set composed of 477 brine samples across the Lithium Triangle. Brine compositions are predominantly of the Cl^- - SO_4^{2-} / Na^+ - Mg^{2+} type, however, major brine chemistry and Li^+ grades vary across the Andean plateau. Brine compositions show some degree of geographic organization but no clear pattern was observed in the Li^+ distribution across the plateau. We highlight an interdependency between the areal surfaces of salt pans and endorheic basins, which, related to Li concentrations, show the following linear proportions: 1) a 1:5 to 1:10 proportionality between the surfaces of basin catchments and those of salt pans; 2) a 2:1 proportionality between maximum and mean Li values; the latter implies that the equation *mean* Li ≈ ½ *max* Li can be employed to predict indicative mean

grades during Li surveys in the Central Andes. In addition, the concentrations of Li can be addressed with respect to the area of salt pans and/or its basin catchments: it would be not only the largest, but also the oldest salars that are expected to hold the greatest Li concentrations. Finally, the area involving all salt pans in the Andean plateau is more than three times the size of what is known as the Lithium Triangle and has a curved crescent shape; we thus propose referring to it in the future as the Lithium Crescent.

Keywords: salt pan; endorheic basin; hydrochemistry; Andes

1. Introduction and historical background

The demand for lithium (Li) has recently known a great increase worldwide due to its application in the fabrication of rechargeable batteries (for mobile phones, personal computers, electric vehicles, etc.). Known global lithium resources involve about 31 Mt, which would represent ~1.50 times the global estimated demand up to the year 2100 (Kesler et al., 2012). Nowadays, lithium is mostly obtained from pegmatite- and brine-type deposits. The former consist of conventional Li mining and represent ~4 Mt (~13%) of estimated resources. Apart from and additional 5 to 6 Mt potential production from hydrothermal solutions and oilfields (Kesler et al., 2012), the remaining ~2/3 (~68%) of global lithium resources are contained in brine-type deposits. This makes them indispensable to meet the growing demand and has caused Li-rich salars to attain the status of an economically, technologically and geopolitically strategic resource (Garrett, 2004; Gruber and Medina, 2010; Mohr et al., 2010; Houston et al., 2011; Kesler et al., 2012; López Steinmetz and Fong, 2019).

Li is a relatively abundant element on Earth with a concentration in the upper continental crust of about 35 ± 11 ppm (Teng et al., 2004). As Li is a very reactive and

geochemical incompatible element, it is commonly present in natural waters as a solute, in its ionic form, Li^+. The mean Li concentration in sea water is 0.18 mg L^{-1} (Riley and Tongudai, 1964), whereas continental waters are characterized by highly variable Li values. Salt pans (salars or salt flats, desert areas where salts accumulate) in arid regions of the globe store brines that contain Li concentrations often averaging two to three orders of magnitude above those in sea water. Most brine-type deposits involve concentrations of more than 400 mg L^{-1} of Li.

The Andean plateau in South America, one of the most peculiar geological features on Earth, has gained a worldwide reputation due to its exceptional Li brine-type deposits (Kesler et al., 2012). The constraints imposed by environmental challenges and the need for strong technological developments to replace fossil fuels are global factors that have driven the Andean Li rush during now more than a decade. Under the effect of the lithium rush, the plateau region became known as "The Lithium Triangle". This was an informal appellation originally designating the area comprised between the Salar de Atacama in Chile (#12 in Fig. 1), the principal Li mine in the world (Moraga et al., 1974; Ide and Kunasz, 1989; Kunasz, 2006), the Salar de Uyuni (#3) in Bolivia to the north (Ericksen and Salas, 1987; Risacher and Fritz, 1991), and the Salar de Hombre Muerto (#43) in Argentina to the south (Godfrey et al., 2013) (Fig. 1). This delimitation of the Andean Lithium Triangle then became established based on the relevance of these three salars, which have been the most important Li spots during the last years. However, there are several more Li-bearing salt pans in this Andean region, many of which located outside of this triangle (Fig. 1). In addition, the nonscientific literature (i.e., diverse press articles, NI reports of mining prospects, etc.) commonly considers all the Andean salt flats as containing significant amounts of Li, although data on brine hydrochemistry, including Li grades, are still quite limited, to this date**.** Therefore, we consider it is important to delimit the area containing all known salt pans. As shown in Figure

1b, such region (in green) corresponds to a curved crescent shape of more than three times the size of the Triangle (in pink), to which we propose referring to as the Lithium Crescent.

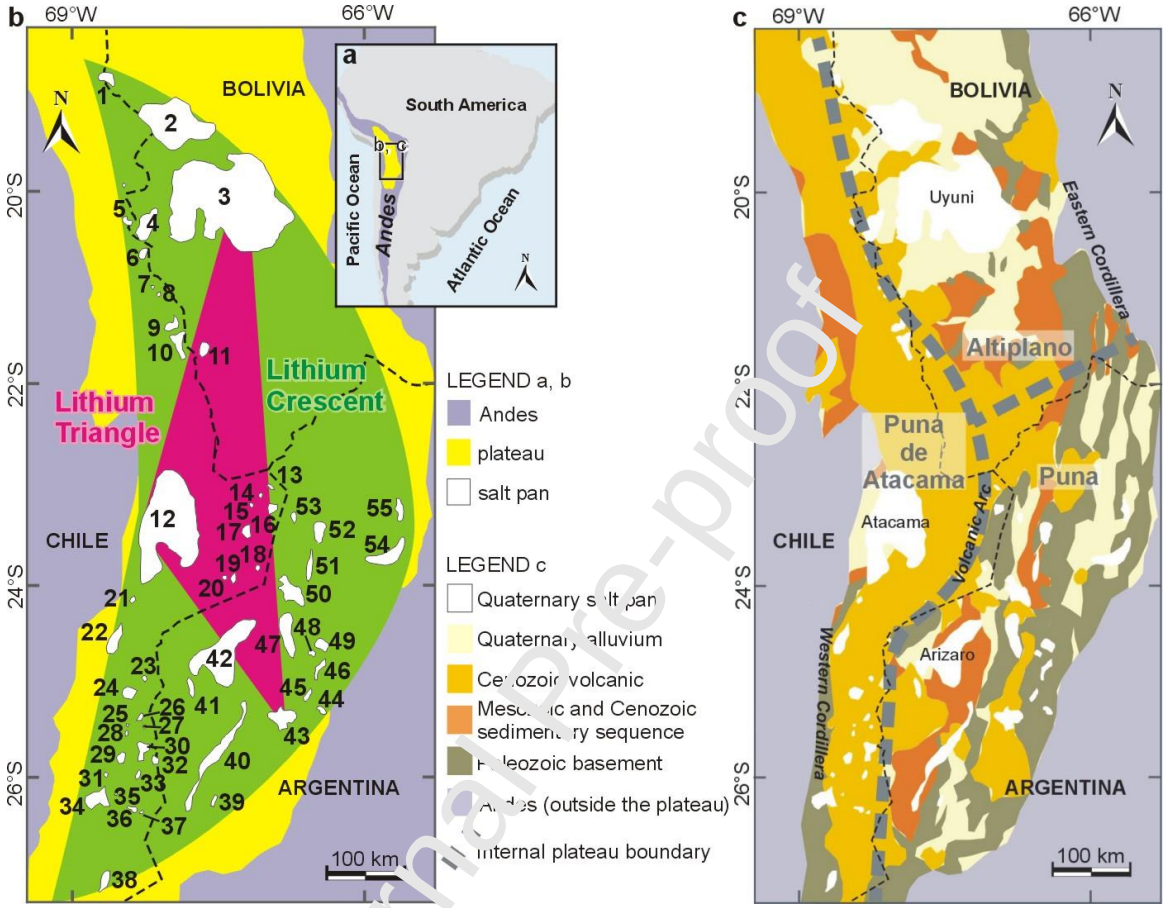

Figure 1. Simplified maps showing the location of a) the Andean plateau and b) salt pans, the Lithium Triangle (pink), and proposed Lithium Crescent (green) corresponding to the area involving all salt pans on the plateau. c) Simplified lithological map of the Andean plateau (modified from Allmendinger et al., 1997), showing the location of the Puna, Puna de Atacama and Altiplano. Dashed black lines represent national borders. Salt pans are numbered in panel b as in Table 1.

The interest for Andean salt pans and their resources began almost a century ago. The first studies were conducted across the Puna de Atacama in northern Chile by geoscientists of the USGS (United States Geological Survey). To this early period of hydrological and geochemical surveys correspond the reports made by Clark (1924), Ericksen (1961, 1963), and Dingman (1967). A few years later, during the 70's, lithium was already perceived as an important resource, as reveals the book "Lithium Resources and Requirement by the year

2000" edited in 1976 by James Vine (also of the USGS). Some of the chapters in this book have become milestone contributions on the topic (e.g., Ericksen et al., 1976b; Kunasz, 1976). During this period, the Chilean State started having an active role on the geological surveying of the Puna de Atacama (the Chilean and western part of the Andean plateau), and on the study of the hydrochemistry of the Salar de Atacama (Moraga et al., 1974; Vila, 1975). Exploration of Andean salars and their Li resources formally began in 1975, when the Chilean State, in association with private companies, conducted the first formal survey of the Salar de Atacama (Kunasz, 1976). Simultaneously, the USGS announced the first results of analyses on two brines samples from the Salar de Uyuni, revealing Li concentrations as high as 490 and 1,510 mg L^{-1} (Ericksen et al., 1976a, 1976b). Since those times, Atacama and Uyuni founded the biggest expectations on the emerging interest in Li-brine type deposits (Mardones, 1986).

The role of the USGS in generating the fundamental knowledge on the hydrochemistry of Andean salt pans, especially in the Puna de Atacama but also in the Bolivian Altiplano (see Ericksen et al., 1977), remained predominant for more than half a century and continued up to the end of the 80's (see Stoertz and Ericksen, 1974; Ericksen and Salas, 1977; Ericksen et al., 1978; Ericksen and Salas, 1987; Ide and Kunasz, 1989). The two following decades were characterized by the acquisition of vast hydrochemical data sets of many Chilean salars (Alonso and Risacher, 1996; Risacher and Alonso, 1996; Risacher et al., 2003) and Uyuni (Risacher and Fritz, 1991; Risacher and Fritz, 2000; Risacher and Frits, 2009; Lowenstein and Risacher, 2009). These new major contributions, which included for example the hydrochemical characterization of more than 170 brine samples across the entire Uyuni (Risacher and Fritz, 1991), were in charge of a French-Chilean council headed by Professors François Risacher of the IRD (Institut de Recherche pour le Development, France) and Hugo Alonso of the UCN (Universidad Católica del Norte, Chile). From this French-Chilean

collaboration emerged the hydrochemical data available today on the Puna de Atacama and Altiplano salt pans, and which remain currently used by COCHILCO (Corporation Chilena del Cobre, the Chilean public society owning mining properties for Cu, Li and other metals in Chile). Additional hydrological and hydrochemical studies, including isotopic assessments in salars and hydrothermal springs in the Puna de Atacama and Altiplano, have been conducted during the last years (e.g., Carmona et al., 2000; Boschetti et al., 2007; Vasquez et al., 2013; Boutt et al., 2016; among others). It was only concurrently to these recent studies that the lithium prospection started along the southeastern side of the Central Andes.

Salars in the Puna (i.e., the Argentine portion of the Andean plateau) have received much less attention that those in the Puna de Atacama and Altiplano. It was probably due to the major attraction caused by the enormous Li resources that stores Atacama (with exceptional Li mean concentrations of 1,400 mg L^{-1}; Moraga et al., 1974; Ide and Kunasz, 1989; Kunasz, 2006), and perhaps also due to the blinding expectations triggered by a salt pan having such a giant dimension as Uyuni (10,580 km^2). It remains that the Puna salt pans stayed almost unexplored up to only a decade ago, despite the recent context of the Andean lithium rush. The first hydrochemical studies were conducted locally on a few salars: the Salar del Rincón (#50; Ovejero Toledo et al., 2009), Salar de Hombre Muerto (Godfrey et al., 2013), Olaroz (#52; Lerda et al., 2016; Franco et al., 2016), Guayatayoc (#55; López Steinmetz, 2017), and the first isotopic data on the Salar de Ratones (#45), Centenario (#46), and Olaroz (Orberger et al., 2015; García et al., 2019; Franco et al., 2020). A broad survey of the Li-bearing salars in the Puna plateau was only recently accomplished, by geoscientist of the Argentine State, who investigated the brine hydrochemistry for the 17 major salars of this part of the Central Andes (López Steinmetz et al., 2018; López Steinmetz et al., 2020a). Because of this long-lasting lack of information, so far it has not been possible to address the hydrochemistry of Andean salt pans in a regional perspective, i.e., in a spatial-geographical

sense, which implies having an overview of all of these salt pans together. Almost a century after the first USGS surveys, the last surveying achievements in the Puna salars finally give us the opportunity of compiling the existing data set and globally assess the hydrochemistry of the Lithium Crescent.

Li-bearing Andean salt pans are exclusively hosted in endorheic basins (isolated hydrological units corresponding to internally drained areas). The onset of endorheism in the Andean plateau established in the Neogene, associated with the creation of orographic deserts within intermontane settings in response to plateau uplift, as well as widespread volcanism (Alonso et al., 1991; Vandervoort et al., 1995; Alonso et al., 2006; López Steinmetz et al. 2020b). The formation of endorheic basins and salt pans is a function of the spatial and temporal distribution of the topographic configuration, sedimentation and erosional processes, as well as climate (Sobel et al., 2003; Hilley and Strecker, 2005; García-Castellanos, 2006; Garreaud, 2009; Tremblay et al., 2015; López Steinmetz et al., 2020b). One might suspect that, under analogous climatic and geological conditions, whichever they may have been, the larger a basin catchment, the larger the size (and volume; i.e. depth) of the salt pan. But because Earth and its processes are typically multi-dimensionally (4D, space - time), heterogeneous and complex (Becker and Braun, 1999; Paola et al., 2009), this relationship cannot be taken for granted. One of the objectives of the present contribution is to address the interdependency between the areal surfaces (size) of salt pans and of their endorheic basins and relate them to Li grades within an Andean perspective. Remarkably, our findings indicate that this size function follows in fact a proportional ratio across the Andean plateau.

No clear geographical pattern in Li distribution (nor concentration) has been found across the Lithium Crescent (López Steinmetz et al., 2020a), except that maximum Li concentrations have been reported from salt pans located in the center of the plateau (Fig. 1). Similarly, consistently with the latest studies on this area (Egenhoff and Lucassen, 2003;

Peralta Arnold et al. 2017; García et al., 2019; Meixner et al., 2019), our observations rule out a geographical control on the primary source of Li (and its concentration), and suggest that a combination of basin-scale processes and endorheic surface sizes control, at least in part, Li grades. It is likely that the lithological characteristics of each salar will have contributed to its geochemical composition. However, to our knowledge, no such study has been carried out yet. Figure 1c shows a synthetic view of lithologies underlying salt pans in the Andean plateau. Any given salar sits on several units, which influence the specific input of the lithology on a salar's chemical signature that are in also probably controlled by more large basin-scale processes like hydrothermalism.

In addition to the salar/basin size function, further objectives of the present contribution are: - to summarize the hydrochemical data sets of brines from salt pans at the Andean scale; - to identify regional patterns (i.e., spatial-geographical) for Li distribution and brine concentrations; - to recognize useful criteria (e.g., hydrochemical, geographical, geomorphological, etc.) for surveying of Li-brine type deposits; - to discuss in absolute and comparative terms the relevance and potential of Andean prospects. A better knowledge of the salars in this region of the Andes and of their Li endowment will necessarily prove beneficial for a better governance of natural resources, whether it be administrative exercise, private sector investment strategies, or simply contributing to the public knowledge.

2. Geology of the Andean Plateau

The Andes display along the western South America (Fig. 1). The Orogenic processes that conducted to the Andes mountain building started in the early Cenozoic after major reorganization of tectonic plates in the eastern Pacific, driving the convergence of the Nazca and South American plates (Tassara, 2005, and references therein).

The Andean plateau (Fig. 1 B) is a tectonic elevation area settled in the Central Andean zone. It occupies parts of northern Chile and Argentina, western Bolivia and southernmost Peru. The plateau involves the internally drained basins of the Central Andes (Allmendinger et al., 1997), which largely correspond to the areas settled above the 3 km elevation contour (Isacks, 1988).

The plateau involves a >60-70 km-thick crust and thin lithosphere (without or with very thin lithospheric mantle, see Allmendinger et al., 1983; Coira et al., 1993; Allmendinger and Gubbels, 1996; Whitman et al., 1996). The plateau is flanked to east and west by morphotectonic units of the continental plate, the Eastern and Western Cordilleras (Fig. 1 C), whereas in the N-S direction the plateau extent coincides with abrupt dip changes along the subduction zone, from flat (<10°) to normal (~30°) subduction, and with the intersection of the Nazca and Juan Fernández oceanic ridges (Kaesara, 2005, and references therein). The Eastern Cordillera reaches 5-6 km elevation and it is a doubly-vergent deformation belt active until the middle-late Miocene (Herail et al., 1996; McQuarrie, 2002). South of 27°S, the tectonic style of the Eastern Cordillera transitions to uplifted basement blocks made of crystalline Palaeozoic rocks and the Sierras Pampeanas (Ramos et al., 2002). The Western Cordillera is an Eocene magmatic and tectonic belt (Mpodozis and Ramos, 1989) that is related to a west-vergent thrust system (WTS, Muñoz and Charrier, 1996). The Western Cordillera has peaks that rise to ~6 Km-in-high and involves stratovolcanoes of Miocene and younger age at the margin of the plateau (Jordan et al., 2010).

The geological characteristics of the Andean plateau vary along-strike. Internal plateau changes on topography, volcanism, tectonic style and subduction conditions, among others relevant aspects, have led to identify major internal plateau subdivisions: the Altiplano (15°-22°S), the Puna (22°-27°S) and the Puna de Atacama (east of the volcanic arc) (Jordan et al. 1983, Mpodozis and Ramos, 1989; Fig. 1 C). The Puna - Altiplano transition occurs at ~22°S.

The Altiplano is characterized by a broad, low-relief, with a mean elevation of ~3.8 km. The Puna lies at an average elevation nearly a kilometer higher than the Altiplano, holds younger mafic magmatism (Maro et al., 2017), and its physiography involves several endorheic depressions bounded by basement-cored ranges (Whitman et al., 1996, Allmendinger et al., 1997, Jordan et al., 2010). The volcanic arc displays nearby N-S and separates the Altiplano-Puna on the eastern side of the plateau from the Puna de Atacama in the west. The volcanic arc (also known as the CVZ, the acronym for Central Volcanic Zone, 15°-28°S) is a chain of Miocene to Quaternary stratovolcanic complexes and andesitic-rhyodacitic domes of high-K calcalkaline affinities (Allmendinger et al., 1997; Kay et al., 1999, Jordan et al., 2010). The Puna de Atacama sets west of this volcanic arc and involves the Atacama basin, a major topographic and geologic anomaly that is one of several anomalous features occurring across the plateau margin at this latitude (Schurr et al., 1999; Götze and Krause, 2002; Belmonte, 2002).

From a stratigraphic point of view, the plateau is filled with synorogenic deposits that record clastic, volcanic, and evaporative Cenozoic episodes (Allmendinger et al., 1997; Baby et al., 1997; McQuarrie, 2002, Alonso et al., 2006). Most of compressive deformation and plateau uplift occurred in the Miocene and Pliocene all together with major felsic magmatism in the region. Large volumes of dacitic ignimbrites (over 104 km^3 erupted volume) erupted from caldera complexes located in and to the east of the arc conducted to Altiplano-Puna plateau to be the largest Neogene ignimbrite province in the world (Babeyko et al., 2002, and references therein).

The plateau basement largely consist of Ordovician, and, locally, older metasedimentary marine, plutonic and volcanic rocks. Basement rocks dominate the outcrop along uplifted ranges. The basement is unconformable overlain by sparse exposures of marine calcareous sequences that record the Cretaceous - Paleocene rift basins. These deposits

correspond to the Salta Group (Brackebusch, 1883, 1891; nom. transl. Turner, 1959) in the Puna and its northwards equivalent Supersequences Puca and Coro-Coro (Sempere et al., 1997) in the Plateau and Western Cordillera of the Bolivian Andes.

Diachronic deformation (Hongn et al., 2007) drove Andean deposition in emergent continental basins. Cenozoic basin fill typically involves red beds, conglomerates and playa deposits containing interlayered evaporites and tuffs. Andean sequences resulted from sedimentation in interconnected and isolated basins during the evolving Andean foreland system (Lopez Steinmetz and Montero-Lopez, 2019, Montero-Lopez et al., 2020, Adad et al., 2020, and references therein). Regional isolation has strengthened once the plateau raised in the Mio-Pliocene. This period was characterized by a flare-up magmatism, regional uplift and the establishment of generalized endorheism (Isacks, 1988; Kay et al., 1994, Allmendinger et al., 1997; Garzione et al., 2008, 2017, Gianni et al., 2020). The plateau rise and the Andean basin formation remain subjects of ongoing debate, as some data seems indicate that the formation of the high plateau, endorheism and intermontane basins could have started together and as early as the Paleogene (Canavan et al., 2014; Scott et al., 2018, López Steinmetz et al., 2020c). Quaternary alluvium covers the low-laying planes between mountain ranges and volcanoes. Halite-dominated pans, locally known as *salares* and *salinas*, formed because of the extremely arid climatic conditions that prevail in these high-altitude endorheic basins since at least the Miocene (Alonso et al., 2006).

3. Material and Methods

The dataset in this article comprises two types of information: 1) major hydrochemistry including Li concentrations in brines from Andean salt pans, and 2) the areal surface (size) of these salt pans and of their basin catchments. The hydrochemical and Li data were obtained by compiling available information for 49 Andean salt pans published in the

scientific literature. All the areal surfaces of salt pan and respective basin catchments were obtained from satellite imagery. These values consist of geomorphological considerations of areal surfaces for 55 salt pans and their basin catchments, which include the 49 salt pans for which Li data were obtained, plus 6 additional salt pans from which there is no available hydrochemical information (i.e., Salar Grande, Capur, Los Infieles, Salar de la Laguna, La Piedra Parada, and Wheelwright). Surface sizes are summarized in Table 1. Salt pan locations are shown in Figure 1 and detailed in Table A1 of the Electronic Supplementary Data.

As detailed in the historical context outlined in Section 1, it is important to realize that the survey of Andean Li has involved a long period of data acquisition and that the available brine chemistry dataset emerged from diachronic sampling campaigns conducted by various scientists during different periods: 1) in most cases, the brine dataset from a particular salt pan results from a unique sampling campaign (i.e., no longitudinal sampling variation data are available), and 2) from a regional point of view (i.e., Andean plateau scale), when comparing the brine chemistry of different salt pans, datasets are composed by diachronic sampling from one salt pan to the other. These aspects imply disparate frameworks for time-dependent conditions that can influence the sampling and analytical methodology. Examples include climate (which controls saline saturation of brines regulating Li concentrations), sampling techniques (which determine the quality and representativeness of sampled brines), advances in analytical methodologies (which define hydrochemical data quality), etc. Therefore, we made sure to be particularly careful when assessing the validity of each dataset included in our regional brine hydrochemistry compilation: we only considered peer-reviewed scientific articles to construct our dataset.

The hydrochemical data compiled in this review (Table 2) correspond exclusively to residual brines from salt pans. Care was taken to exclude values from springs, rivers or streams from the dataset. In most cases, samples correspond to shallow and sub-surface brines

that were collected from hand-dug pits in the salt pans, i.e., at depths less than 1 m. In a few cases, samples were taken directly from brine pools (i.e., ponding brines) that had formed naturally in the salars (Risacher et al., 199; Lopez Steinmetz et al., 2018; 2020). Data considered for the Uyuni and Coipasa salars, in addition to near-surface brines, consists also of a collection of samples obtained at depths of up to 10 m from 40 holes dug in the salt crust of these salars. In Table 2, the sampling depths (in centimeters) are indicated by numbers in names of the 176 samples from Uyuni and Coipasa (for more details see Risacher and Fritz, 1991). Due to the regional scale of this review and, as just mentioned, the fact that most considered brines come from sampling within the salt pans, the specific location and depth of each of the 477 brines constituting our dataset (Table 2) are not reported here. In Table 2 all samples are grouped by salt pans which are located in Figure 1 and whose coordinates are provided in Table A1 of the Electronic Supplementary Data. In the following lines of this section, all references are provided to the scientific literature considered, as well as details on criteria for building the dataset. For further information on the sampling and analytical techniques deployed for specific data or the specific location of each sample, the reader is referred to the original papers from where the datasets were taken.

In this review, salt pans are grouped into Altiplano, Puna de Atacama and Puna salars, which is roughly equivalent to say Bolivian, Chilean and Argentinian, respectively, given that national borders follow natural boundaries in the plateau (Fig. 1). Readers that are not familiar with Andean geography, can find more detailed discussion on Andean salt pans and brine chemistry in the references listed in the following paragraphs.

The hydrochemical data set (Table 2) involves 477 brines samples and is composed of:

- 178 brine samples from the Altiplano salt pans that majorly correspond to data published by Risacher and Fritz (1991), and to a minor extent by Ericksen and Salas (1987),

- 126 brine samples from the Puna salt pans (Ericksen and Salas, 1987; López Steinmetz, 2017; López Steinmetz et al., 2018; García et al., 2019; López Steinmetz et al., 2020a), and
- 173 brine samples from the Puna de Atacama salt pans reported by Moraga et al. (1974), Vila (1975), Ericksen and Salas (1987), and Risacher et al. (1999; summarized by COCHILCO, 2013).

For the case of the Salar de Atacama, we used samples ATA_0 and ATA_{do}, ATA, and Do1 to Do5 reported for Moraga et al. (1974) and Ericksen and Salas (1987), and ATA-05 and ATA-22 reported by Risacher et al. (1999), which are - to the best of our knowledge - the only available published data on brine samples collected within this salt pan, and offering a complete spectrum of major ions, Li, and TDS. It is important to note that Li values that are either i) isolated, from incomplete ionic characterizations, or ii) from non-scientific reports, were not taken into consideration. According to these criteria, the considered Li values are the unique, scientific published data of brine samples available from samples collected in the Andean salt pans, and offer a complete hydrochemical spectrum. Data reported in other scientific works correspond to inflow waters and/or hydrothermal springs, and not to residual brines lying within these salt pans, and/or do not offer a complete spectrum including TDS, major ions, and Li (i.e., Ericksen et al., 1976a, 1976 b; Crespo et al., 1987; Rettig et al., 1987; Scandiffio and Alvarez, 1990; Scandiffio and Rodriguez, 1990; Mardones and Chong, 1991; Bevacqua, 1992; Garcés et al., 1996; López et al., 1996; Carmona et al., 2000; López Julián et al., 2001; Risacher et al., 2002; Banks et al., 2004; Vinante and Alonso, 2006; Boschetti et al., 2007; Ovejero Toledo et al., 2009; Salas et al., 2009; Schmidt, 2010; An et al., 2012; Durán Iriza, 2012; Vásquez et al., 2013; Boutt et al., 2016; Corenthal et al., 2016; Munk et al., 2018; Godfrey and Alvarez-Amado, 2020).

Mean brine compositions were computed from the information available, summarized in Table 3. In the case of the Salar de Atacama, we also considered values of 1,400 and 6,400

mg L^{-1} as the representative mean and maximum Li concentrations of the Atacama brines, respectively, as listed in Moraga et al. (1974; see also Ide and Kunasz, 1989; Kunasz, 2006). Accordingly, the hydrochemical and Li^+ concentrations of the Atacama brines (i.e., mean and maximum of 562 and 1,570 mg L^{-1}, respectively) from Moraga et al. (1974), Ericksen and Salas (1987), and Risacher et al. (1999) are used for general characterizations such as shown in Figures 2 to 6, however, we used the 1,400 and 6,400 mg L^{-1} mean and maximum Li concentrations when assessing this major salar in its regional context (Figs. 9 and 10). Li maximum (*max*) and mean concentrations of Li^+ and Mg^{2+} in all salars (Table 4) are also considered and discussed. Saturation indexes (SI) at standard ambient temperature and pressure (SATP, 25°C, 1 atm) were computed using the Phreeqc 3.6.2 software, to address the saturation state of brines with respect to main salts. The most representative ranges of SI values are reported in the Results section.

4. Brine hydrochemistry across the Lithium Crescent

4.1. *Altiplano salars*

A few salt pans occur in the southern Bolivian Altiplano. Amongst these salars, the most prominent are Uyuni and Coipasa (#2): with an area of 10,000 km^2, Uyuni is by far the largest salt pan on Earth, and with its 1,650 km^2 Coipasa is the fourth largest salar in the Andean plateau (Fig. 1, Table 1). Empexa (#4 in Fig. 1) and Pastos Grandes (#11) also are large salars with their 402 and 124 km^2, respectively. These salt pans are located at altitudes >3.60 km asl, and their catchments involve endorheic basins having disparate surfaces that range between 600 and 45,200 km^2 (Table 1). None of these salt pans is yet being mined for lithium.

The brine chemistry of Uyuni and Coipasa was thoroughly described by Risacher and Fritz (1991), whereas only two isolated samples are available from Empexa and Pastos Grandes (Ericksen and Salas, 1987; Table 2). The Altiplano salt pans contain highly saline brines with mean TDS (Total Dissolved Solids) values comprised between 123 and 321 g L^{-1} (Table 3), although in most cases TDS are in a range from 100 to ~220 g L^{-1} (Risacher and Fritz, 1991; Table 2). The maximum TDS values reported are of 351 g L^{-1} and 368 g L^{-1}, respectively from Uyuni and Coipasa (Ericksen and Salas, 1987).

Based on their major chemical compositions, brines in Uyuni are of the Mg^{2+} - Na^{+} / Cl^{-} - SO_4^{2-} type, with $Mg^{2+} \geq Na^{+}$, whereas in Coipasa, Empexa and Pastos Grandes brines are of the Na^{+} - Mg^{2+} / Cl^{-} - SO_4^{2-} type, with $Na^{+} > Mg^{2+}$ (Figs. 2 and 3 a). Main characteristics of brines from Altiplano salars are their high Mg^{2+} concentrations and their relatively low K^{+} and Ca^{2+}. Stoichiometric ionic ratios between Na^{+} and Cl^{-} are consistent with the equilibrium solubility of halite for a certain number of the Uyuni brines (i.e., SI ≈ 0, e.g., samples RA130, RB180, RC120), however, a large number of them plot along an oblique line with respect to the 1:1 proportion (Fig. 3 b), suggesting that the brine reached saturation with respect to (and thus precipitated) halite (SI > 0 and up to 0.36, e.g., samples RX10, RZ1, CA150). Except for some samples from Coipasa (e.g., CB150 and CA250), the fact that the SO_4^{2-} : Mg^{2+} ratio forms a trend $Mg^{2+} > SO_4^{2-}$ perpendicular to the 1:1 line, is in turn consistent with the saturation of the brines with respect to epsomite ($MgSO_4\ 7H_2O$, SI > 0 and up to 0.73, e.g., samples RZ1, RT15, RX10), and/or other Mg-bearing sulfated salts (Fig. 3 c).

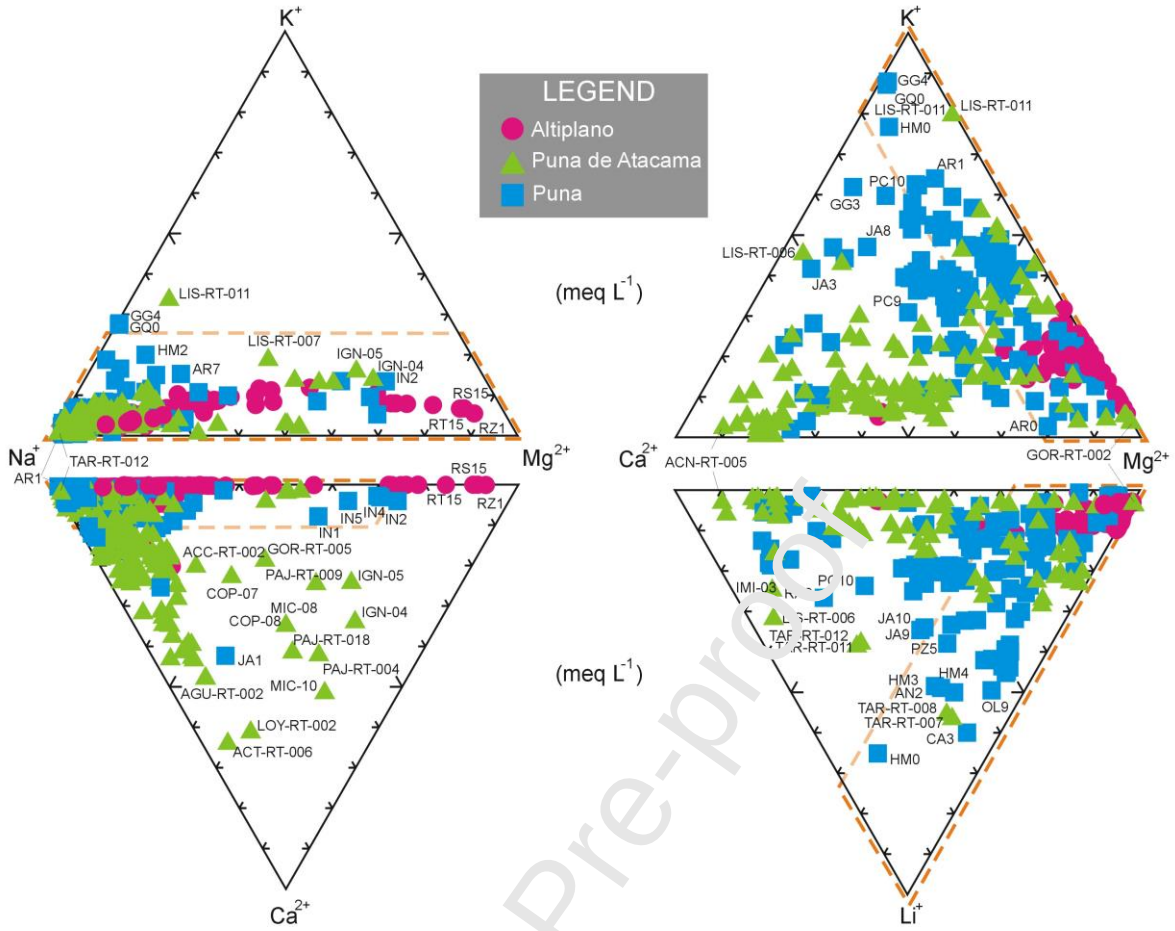

Figure 2. Ternary diagrams displaying relative cationic concentrations measured in brines from Andean salars. Plotted samples and concentrations correspond to those detailed in Table 2. Fields delimited by orange dashed line represent the hydrochemistry of brines from the Tibet Plateau (Li et al., 2019b).

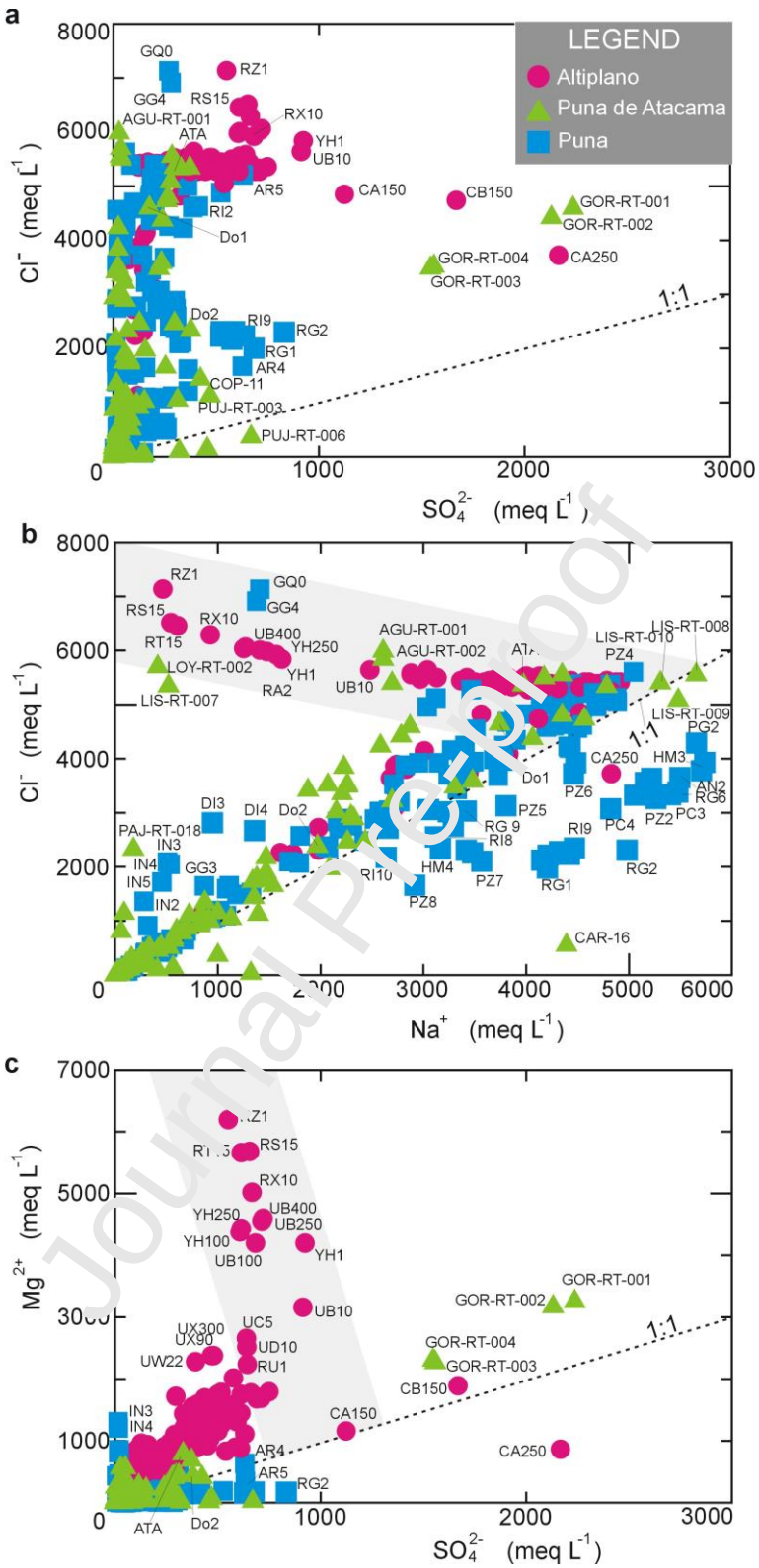

Figure 3. Scatter diagrams plotting the concentrations of a) SO_4^{2-} versus Cl^-, b) Na^+ versus Cl^-, and c) SO_4^{2-} versus Mg^{2+} in brines from Andean salars. Gray zones in panels a) and b) signal trends that are independent from the 1:1 ratio (dashed line) and that could correspond to brine saturation. Plotted values correspond to concentrations detailed in Table 2.

The mean Li^+ concentrations in Empexa and Coipasa are 213 and 258 mg L^{-1}, respectively, whereas the only available sample from Pastos Grandes indicates Li values as high as 1,640 mg L^{-1} (Ericksen and Salas, 1987). In Uyuni the maximum reported Li value is of 4,720 mg L^{-1} with a mean of 715 mg L^{-1} (Risacher and Fritz, 1991; Tables 2 and 3). Two different tendencies are observed between the concentrations of Li^+ and Cl^- in the Altiplano brines: an oblique trend, which only includes a part of the Uyuni's brines, suggests a positive correlation between Li^+ and Cl^-, whereas a horizontal trend including samples at higher Li values, shows that the concentrations of Li^+ in most samples evolve independently from those of Cl^- (Fig. 4 a). Two different tendencies are also observed between Li^+ and Na^+ (Fig. 4 b). A certain amount of data from Uyuni form a roughly positive Li^+ versus Na^+ correlation. This trend is consistent with the correlation observed between Li^+ and Cl^-, and together suggest that the concentrations of Li^+ could be related to the equilibrium solubility of halite. Furthermore, the Pearson's correlation coefficient (R) corresponding to the mean concentrations of Li^+, Cl^- and Na^+ across Andean salars ranges between 0.70 and 0.80 (Fig. 5). The second tendency depicted by the Li^+ versus Na^+ data trend includes most of the Altiplano brine samples, and forms an oblique line showing Li^+ increasing inversely to Na^+, up to the concentrations of Uyuni samples RS15 and RZ1 (Figure 4 b). This pattern, which most likely corresponds to brine saturation with respect to halite, suggest that the Li^+ concentrations increase while halite precipitates.

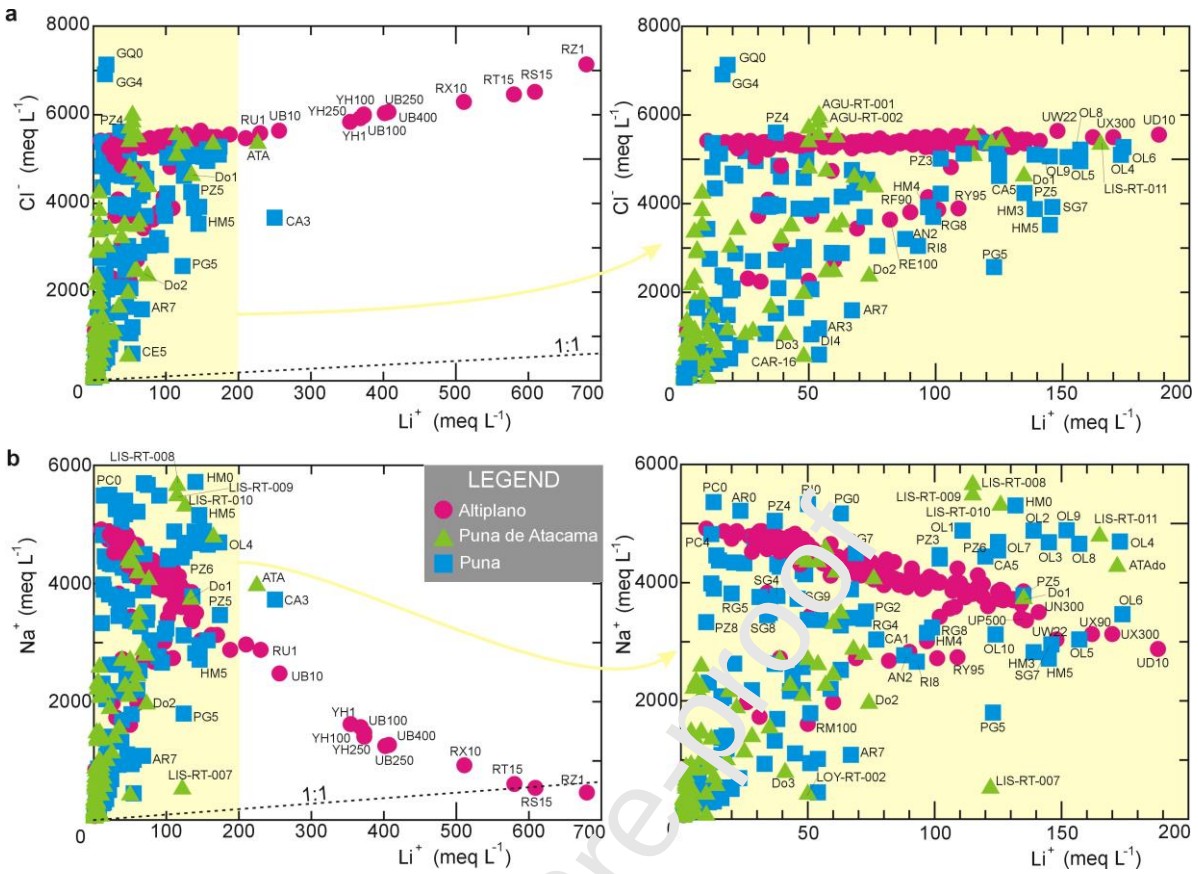

Figure 4. Scatter diagrams showing the variations of a) Li^+ versus Cl^-, and b) Li^+ versus Na^+, in brines from Andean salars. Insets (yellow panels) offer a detailed view of the data displayed in the yellow boxes. Plotted values correspond to the concentrations detailed in Table 2.

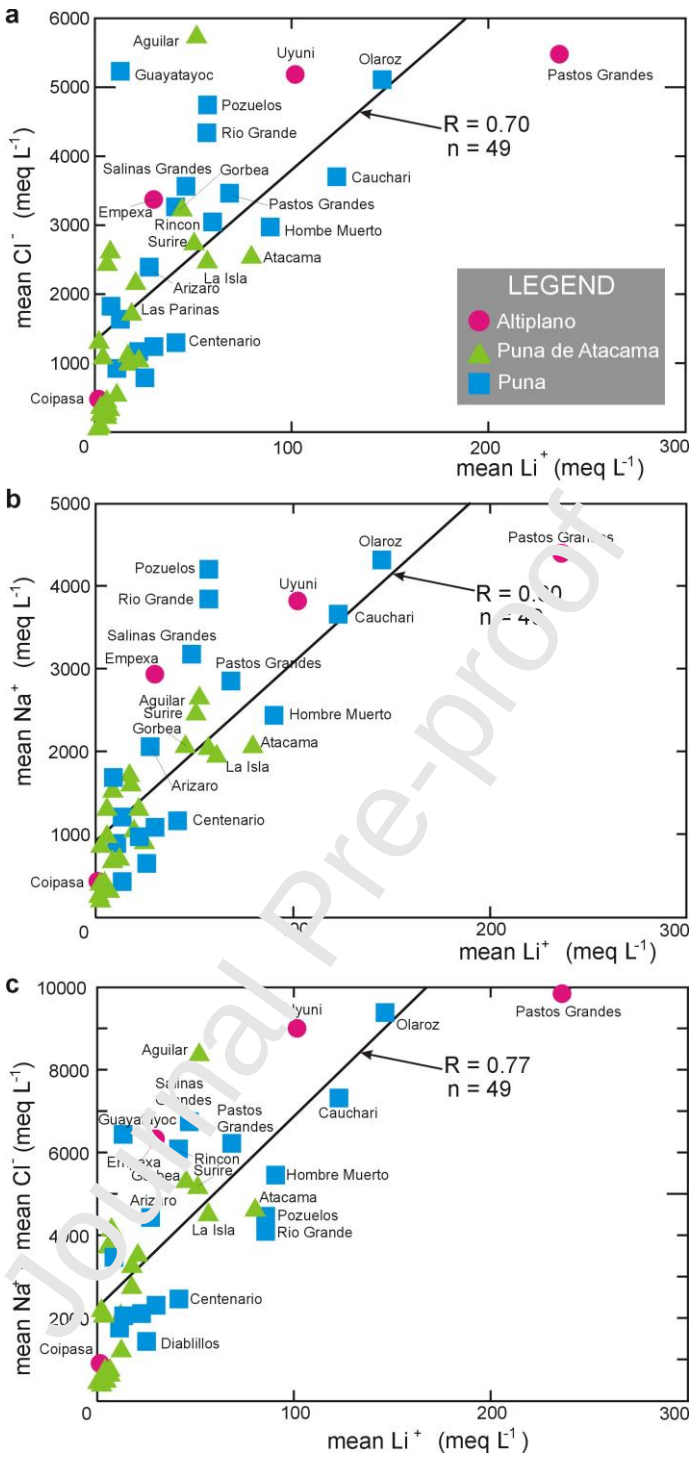

Figure 5. Scatter diagrams plotting the variations for the mean concentrations of a) Li^+ versus Cl^-, b) Li^+ versus Na^+, and c) in Li^+ versus $Na^+ + Cl^-$, in the Andean salars according to values presented in Table 3. The plotted mean Li^+ concentration for Atacama results from considering values reported by Moraga et al. (1974), Ericksen and Salas (1987), and Rischaer et al. (1999). It is important to note that this value differ from the globally accepted mean Li concentration in Atacama that is 1,400 mg L^{-1} (~202 meq L^{-1}; Moraga et al., 1974; Ide and Kunasz, 1989; Kunasz, 2006). R is the Pearson correlation coefficient, n is the total number of points in the data set (i.e., the number of salars).

An additional interesting feature of the Altiplano brines is that Li^+ also seems to correlate, in different proportions, with K^+, B, and Mg^{2+} (Fig. 6). The K^+:Li^+ ratios in most Altiplano brines array along a 1:4 trending line, a pattern that could be consistent with the equilibrium solubility of 1:4 salts (complex K-, Li-, Na- Cl salts, yet undetermined). Samples plotting along an oblique trend to the 1:4 proportion suggest saturation of the brine with respect to these compound (Fig. 6 a). When comparing mean values, it can be observed that the correlation R between Li^+ and K^+ reaches 0.68, which confirms this pattern reflects a Li^+ - K^+ interdependency (Fig. 6 b).

The concentrations of Li^+ and B in the Altiplano brines plot along a line that defines a 3:1 proportion trend (Fig. 6 c), and mean values are highly correlated (R = 0.78; Fig. 6 d). The concentrations of Li^+ also increase consistently with those of Mg^{2+} (Fig. 6 e), with the Mg^{2+}:Li^+ ratios defining trends with correlations of about 1:50 in Coipasa, 1:13 in Empexa and Uyuni, and ~1:1 in Pastos Grandes (Fig. 6 e). The observed proportionalities between Li^+, B and Mg^{2+} have not been yet explained, and could correspond to the equilibrium solubility of complex borates and other salts or, alternatively, to the ionic influence of cations in exchangeable positions within clays. In any case, these proportionalities require further investigations. Interestingly, the Li^+ versus B pattern defined by the Altplano brines is close to that displayed by brines from saline lakes in the Tibet Plateau (Fig. 6 c), which contains the second most important Li-brine type deposits on Earth (Zheng and Liu, 2009; Kesler et al., 2012; Li et al., 2019b, and references therein).

Mean Mg:Li ratios are 22 in Uyuni, 40 and 47 in the Empexa and Coipasa, respectively, and as low as 2 in Pastos Grandes (Fig. 6 C, Table 4). With Mg^{2+} means of >15,000 and >12,000 mg L^{-1}, the Uyuni and Coipasa brines contain amongst the highest magnesium concentrations in the Andean plateau (Figs. 2 and 5 e, Tables 3 and 4).

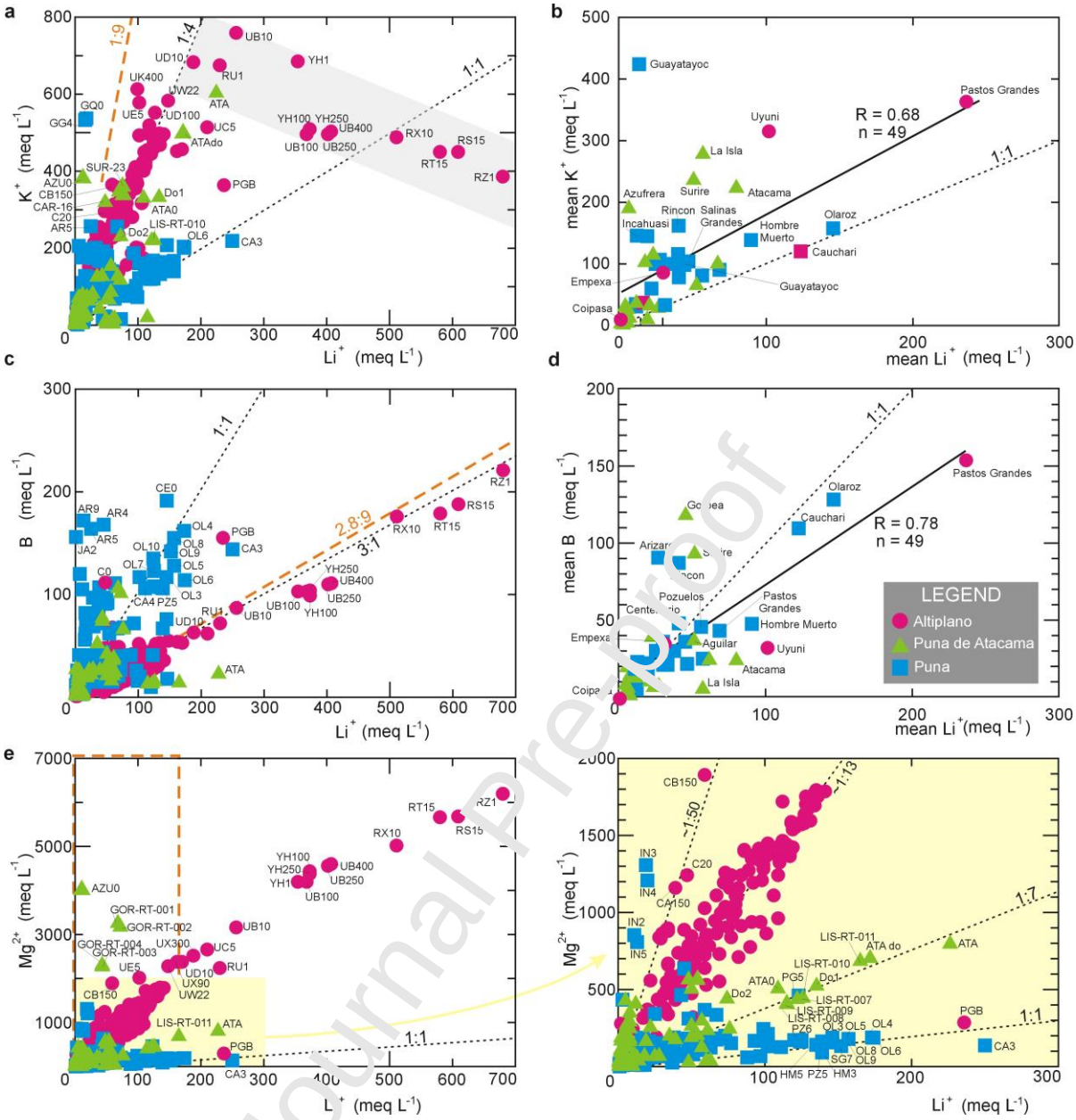

Figure 6. Scatter diagram showing the variation between the concentrations of a) Li^+ and K^+, b) mean Li^+ and mean K^+, c) Li^+ and B, d) mean Li^+ and mean B, and e) Li^+ and Mg^{2+}. Values plotted in a), c), and e) are for brine compositions presented in Table 2. Scatter diagrams b) and d) plot mean concentrations according to values summarized in Table 3. Continuous line: R correlation coefficient, with n = the total number of salars. Dashed line: stoichiometric ratio. Orange dashed line and rectangle: stoichiometric proportions (panels a and c) and field (panel e) characterizing brines from the Tibetan Plateau (data from Li et al., 2019b).

4.2. *Puna de Atacama Salars*

Salt pans in the Puna de Atacama are located at altitudes between 2,300 (Atacama) and 4,500 (Pujsa, #15) m asl (Table 1, Fig. 1). The surfaces of these salars and their endorheic

basins are highly variable. With its 3,000 km^2, Atacama is the largest Chilean salt pan and, with a catchment area of 18,100 km^2, also the largest endorheic basin in the Chilean portion of the plateau. The smallest salt pans, such as Salar de la Laguna (#35) and Ignorados (#27), are only of 1 km^2 (Table 1). In the Puna de Atacama, only the Salar de Atacama is presently being mined for Li.

The brine chemistry of salars in the Puna de Atacama was comprehensively addressed by Risacher et al. (1999). Brines have highly variable salinity, with TDS ranging up to 370 g L^{-1}. The highest salt concentrations are observed in brines from Sunire (#1), Atacama, and La Azufrera (#25), where mean values grade between 178 and 267 g L^{-1} (Tables 2 and 3).

According to their major chemical compositions, the Puna de Atacama brines are of the Na^+ - Mg^{2+} / Cl^- - SO_4^{2-} type (Figs. 2 and 3 a). A few brines contain $Mg^{2+} \geq Na^+$ (e.g., samples IGN-04 and 05, PAJ-RT-004 and 018, ACT-RT-006; Fig. 2), and/or $Ca^{2+} \geq Na^+$ and Mg^{2+} (e.g., samples ACT-RT-006, LOY-RT-002, MIC-10, and AGU-RT-002; Fig. 2). The concentrations of Cl^- are generally higher than those of SO_4^{2-}, with few samples of low salinity having $SO_4^{2-} > Cl^-$ (e.g., samples PUJ-RT-006 to 008, ACSS-RT-005 to 007, IGN-004 and 005; Fig 3 a). The main characteristics of salar brines in the Puna de Atacama are their high Ca^{2+} and their relatively low K^+ when compared to brines from neighboring parts of the plateau (Fig. 2).

The Na^+ versus Cl^- concentration patterns are quite similar to those observed in the Altiplano brines (Fig. 3 b). Stoichiometric ratios ~1:1 between Na^+ and Cl^- are consistent with the equilibrium solubility of halite (SI ≈ 0, e.g., sample Do2; Fig. 3 b), and samples plotting oblique to the 1:1 proportion trend suggest brine halite saturation and precipitation (SI > 0 and up to 0.47, e.g., samples AGU-RT-001, LOY-RT-002, LIS-RT-007; Fig. 3 b). Similarly to the Altiplano brines, the SO_4^{2-} and Mg^{2+} concentrations plot along the 1:1 proportional line, which is consistent with the equilibrium solubility of epsomite ($MgSO_4$ $7H_2O$), and/or other

Mg-bearing sulfates (Fig. 3 c). However, some brines do not match the SO_4^{2-}:Mg^{2+} uniequivalent proportion trend, which implies the presence of other salts that are not in equilibrium with the brines (e.g., SI maxima for anhydrite and gypsum reach values of 1.07 and 1.10, respectively, in sample AGU-RT-001).

Li concentration in pan brines of the Puna de Atacama are very high. Indeed, the Puna de Atacama desert is known as having the richest Li brine-type deposits on Earth, and the salt pan of Atacama is the most important operating Li mine in world today, with mean Li grades of 1,400 mg L^{-1} and maximum measured concentrations reaching 6,400 mg L^{-1} (Moraga et al., 1974; Ide and Kunasz, 1989; Kunasz, 2006). Other than Atacama, high Li^+ concentrations were also measured, for instance, in La Isla (#30), Gorbea (#26), and Surire, where mean Li^+ grades are between 300 and 400 mg L^{-1} (Tables 2 and 3).

Despite that the Li^+ versus Cl^- and Na^+ concentrations distribute quite dispersedly, samples plot within the field defined by trends of the Altiplano brines (Fig. 4). Furthermore, mean Li^+, Cl^- and Na^+ concentrations from the Puna de Atacama salars match the correlation lines characterizing other Andean brines (Fig. 5). Positive correlations could also exist between the concentrations of Li^+ and K^+ (Figs. 6 a and b). However, no evident correlation is observed between Li^+ and B (Figs. 6 c and d), whereas some samples arrays along the 1:7 proportional line, which might imply the existence of complex Li, Mg bearing salts (Fig. 6 e).

Despite that nearly uniequivalent proportions of Mg and Li are found in El Tara (#13) and Imilac (#21), these ratios are most often ≠ 1. Mg^{2+}:Li^+ ratios <10 are observed in Pujsa, Loyoques (#16), La Isla, Las Parinas (#32), Surire, Maricunga (#38), and Atacama, whereas brines with Mg^{2+} concentrations about two orders of magnitude higher than those of Li^+ are found in Michincha (#7), Ignorados, and La Azufrera (Fig. 6 e, Table 4). This kind of brines, characterized by Mg^{2+} >> Li^+, are also observed in brines from saline lakes in the Tibet Plateau (Fig. 6 e; Li et al., 2019b).

4.3. *Puna Salars*

The Puna plateau holds 17 major salars that are located at altitudes ranging between 3,269 (Incahuasi, #39) and 4,080 (Jama, #53) m asl (Table 1; Fig. 1). With the exception of giant Arizaro (1,708 km^2, #42) and the three smallest salars sizing less than 10 km^2 (Centenario, Diablillos, #44, and Ratones), salt pans surfaces range from 30 to 650 km^2 (Table 1). These salars are settled in endorheic basins with surfaces that mostly vary from 1,000 to 9,000 km^2. With 14,536 km^2, Rio Grande (#41) holds the largest basin catchment area, whereas the smallest basins correspond to the smallest salt pans (Table 1).

Amongst the Puna salt pans, only Hombre Muerto and Olaroz are being actively mined for Li. The brine chemistry in the Puna salars has been characterized by López Steinmetz et al. (2018) and López Steinmetz et al. (2020a). These brines contain highly variable saline content and ionic proportions. TDS as low as 6 g L^{-1} have been found in some salars such as Jama, whereas TDS up to 381 g L^{-1} were found at Olaroz, define the maximum measured values (García et al., 2019). Brines from the Puna salars are of the Na^+ - K^+ / Cl^- - SO_4^{2-} type in the north, of the Na^+ - Mg^{2+} / Cl^- - SO_4^{2-} type in the south, and the SO_4^{2-} concentrations increase from south to north (Figs. 2 and 3 a).

Similar to the Altiplano and Puna de Atacama, most of the Puna brines have Na and Cl concentrations that correlate positively along a 1:1 stoichiometric ratio, which is consistent with equilibrium solubility of halite (SI ≈ 0, e.g., samples AR9, PC7; Fig. 3 b). Some degree of correlation could exit between SO_4^{2-} and Mg^{2+} in some samples such as AR4 and AR5. However, as depicted in Figure 3 c, the Mg^{2+}:SO_4^{2-} ratios do not match the 1:1 trend, implying the existence of other Mg^{2+}- and SO_4^{2-}-bearing salts (e.g., maximum SI values for anhydrite and gypsum range from -3.19 to 0.54 and -2.95 to 0.63, respectively, in samples IN3 and RG2).

Amongst Puna salars, maximum Li^+ values of 1,739 and 1,213 mg L^{-1} were found in Cauchari and Olaroz, respectively (Tables 2 and 4). In addition to these salt pans, where mean Li concentrations reach 860 and 841 mg L^{-1}, respectively, high Li-graded brines are stored in Hombre Muerto, Pastos Grandes (#49), Pozuelos (#48), Rio Grande, Salinas Grandes, and Rincon (#50), where mean Li^+ concentrations are between 280 and 570 mg L^{-1} (Table 3).

According to its geochemical behavior, Li variations in brines are expected to be consistent with those of other conservative solutes such as Cl^- and Na^+. Positive correlations can exist between the concentrations of Li^+, Cl^- and Na^+ in some cases (Figs. 4 and 5). Furthermore, Li also seems correlate positively with K^+ and B, and to a minor extent also with Mg^{2+} (Fig. 6). Interestingly, the concentrations of Li^+ and K^+ in the Olaroz and Cauchari (#51) brines display along the 1:1 ratio, whereas proportions in the remaining brines better fit the 1:4 dominant pattern defined by the Uyuni's brines (Figs. 6 a). Despite there is no clear pattern between Li^+:B and Li^+:Mg^{2+}, nearly equivalent proportions are mainly observed in salt pans from the northern Puna (Figs. 6 c, d and e). However, brines from the Southern Puna instead show ionic proportional patterns mainly displaying parallel to the vertical axis (i.e., parallel to the B and Mg^{2+} axes), such as for Incahuasi, which brines match the trend ~1:50 ratio of the Coipasa brines (Fig. 6 e).

With the exception of Incahuasi, which brines contain high Mg^{2+} concentrations that are in the range of those observed in Uyuni and Coipasa (Fig. 6 e), remaining Puna salt pans, especially in the northern Puna, show the lowest Mg^{2+} values amongst the entire Andean plateau (Fig. 2, Table 4). These salars are characterized by brines having mean Mg:Li ratios ≤ 11, and some brines have exceptionally low ratios of 1 to 3, as the case of Ratones, Guayatayoc, Cauchari, and Olaroz (Table 4).

5. Discussion

5.1. Lack of Li geographical distribution

Andean Li-brine type deposits are found both in mature and in immature salars (Houston et al., 2011; Fig. 7 a and b). Andean mature salars, such as Atacama, correspond to halite dominated pans, whereas immature salars, like Uyuni and Olaroz, are mostly filled by clastic saline muds (Houston et al., 2011). Sometimes, mature and immature zones can be found in the same salt pan. For example, western Hombre Muerto corresponds to a mature pan, whereas its eastern side is an immature salar. An additional example is the Salar de Atacama. Here, the halite nucleus (i.e., mature salar) spreads for an area of 1,100 km^2 and ~1,000 m depth, in the southern part of the salar, whereas the northern part is clastic dominated and gypsum rich (Boutt et al. 2016; Corenthal et al. 2016; and references therein).

However, the more often, Andean salt pans are complex combinations of crystalline salt layers, which are interbedded, in highly and variable proportions, with clastic fine -graded sequences (e.g., Salar del Rincon and Maricunga). In the practice, the predominant type tendency of a salt pan is revealed the more clearly during the brine extraction. Pumping in mature and immature pans implicates different responses of the water (i.e., brine) table due to the contrasting porosity (and permeability) of the substrate (i.e., porous salt pan and impermeable clay and muddy -rich deposits, respectively). During operations, pumping in a mature salar conduces to the development of a shallow depression cone of the water table around the pumping well, whereas in immature salars the cone deepens faster than it extends horizontally (Houston et al., 2011).

Three major noteworthy observations need to be addressed concerning mature and immature salars. Firstly, there is no strict rule and the areal extent of mature salars does not necessarily exceed that of immature salars (see Table 1). Secondly, brines in halite-dominated pans does not always contain higher Li concentrations than immature salars (Houston et al.,

2011; see Table 3). Thirdly, high Li -graded brines are not necessarily related to saline nucleus. Furthermore, deeper brines are not systematically richer in lithium. For instance, in the salt pan of Atacama the Li concentration isopleths form a pattern consisting of concentric Li grade zones with maximum values located in the southern part – and not in middle – of the halite nucleus (Moraga et al. 1974; Stoertz and Ericksen 1974; Ide and Kunasz 1989; Bevacqua 1992; Alonso and Risacher 1996; Carmona et al. 2000; Boschetti et al. 2007; Boutt et al. 2016; Corenthal et al. 2016). These concentric patterns are not the same at near surface levels as they are at depth. For example, if it is true that in the Uyuni salar Li concentrations increase concentrically and asymmetrically with depth, moving southward (Risacher and Fritz 1991; Fig. 7 c), in certain parts, Li concentrations do not change with depth, such as along the UI well where a constant Li concentration (300 mg L^{-1}) is reported from near surface down to 10 m depth (Fig. 7 c). An additional example of this is the Salar de Olaroz. The highest near surface concentrations of Li occur forming a pattern that can be followed along a NE-SW axis running through the middle of the salar (García et al., 2020; Fig. 7 d). Conversely, the pattern at ~200 m depth consists of two high Li level zones in the northern and southern parts of the salar, disrupted by an intermediate brine grade zone near the center of the pond (see García et al., 2020; Fig. 7 e).

Aridity is an important parameter controlling brine Li concentration along a vertical profile. By enhancing evaporation near the surface, it can cause shallower brines to have higher Li levels than those lying below. Clearly, a complex interplay of the above aspects to which add other factors such as the presence of hydrothermal springs and the role played by structures on Li-rich waters supply into the system, among many others listed by Godfrey et al. (2013; cf. also discussion below, sections 5.4 and 5.5), drive the singularity of each Andean salar. This notwithstanding, it is remarkable to observe that the major hydrochemical composition of brines is relatively similar across the Andean plateau (Fig. 8).

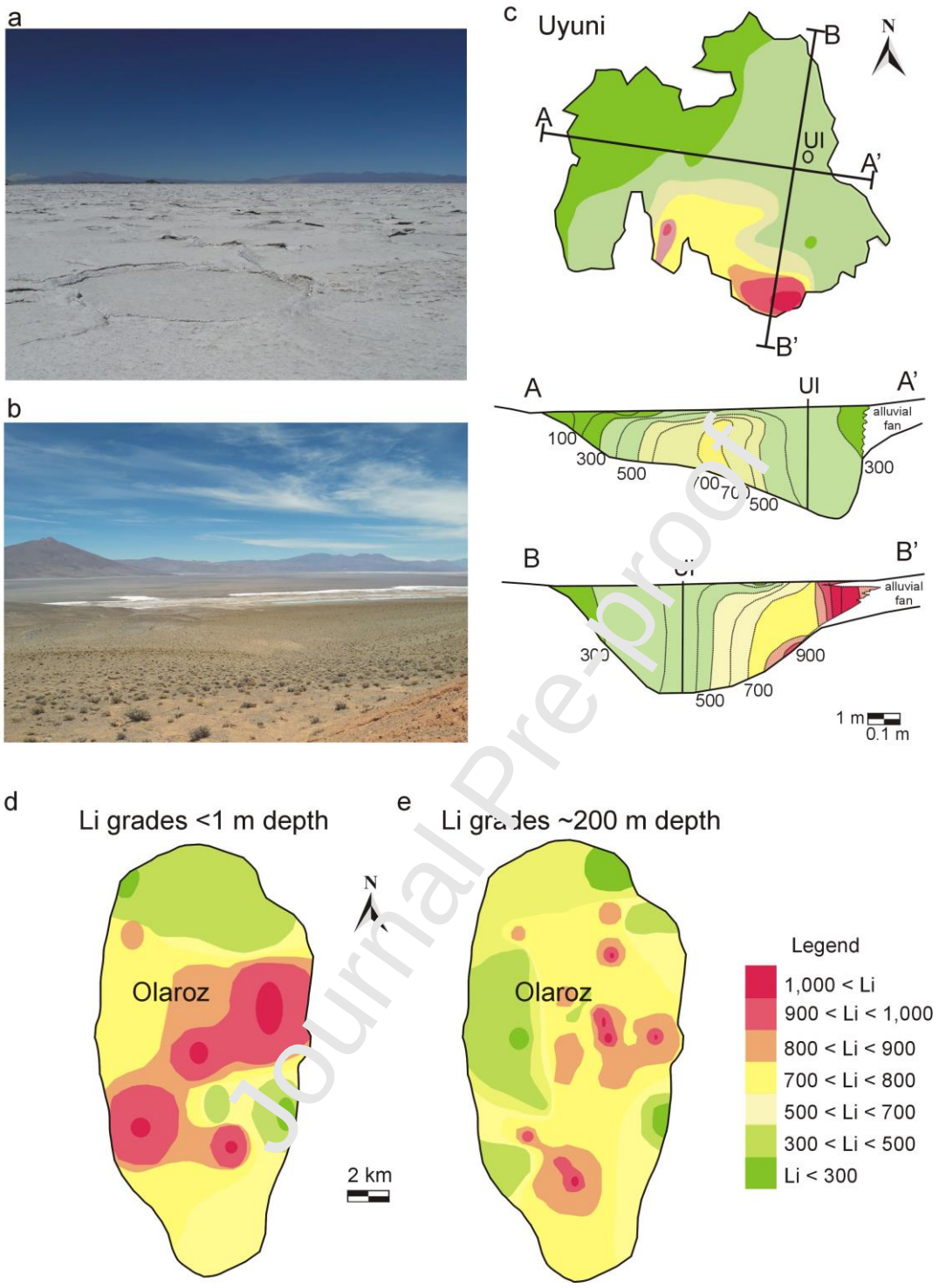

Figure 7. Pictures showing a) Salar de Pastos Grandes (Puna), and b) Salar del Rincón, respectively examples of mature and immature Andean salars. Notice the salt crust and the brown clastic surfaces. c) Map (upper panel) showing the Li isoconcentration curves in brines and the location of vertical profiles A-A' (middle panel) and B-B' (bottom panel) from Uyuni (modified from Risacher and Fritz, 1991). The location of well UI (referred in the text of section 5.1) is shown in panels. d and e) Map showing the concentration of Li in near surface (<1 m depth) and deep (~200 m depth) brines in Salar de Olaroz (modified from Garcia et al., 2020). Li concentrations are in mg L^{-1}.

A typical feature of evolved (evaporated) and highly saline waters is a composition marked by the presence of Cl^- and SO_4^{2-}, and a depletion in CO_3^{2-}/HCO_3^- (Langbein, 1961; Hardie and Eugster, 1970; Eugster, 1980). Andean brines can be compared to those from Li-bearing saline lakes in the Tibetan Plateau (Li et al., 2019b, and references therein), despite obvious geological-environmental differences. In both cases, they commonly belong to the Cl^- - SO_4^{2-} type, and the hydrochemical variability is generally marked by variations in the major cations (Figs. 2 and 3 a). Our data compilation indicates that composition with a Na^+ - Mg^{2+} signature largely predominate in the whole Andean plateau (and in Tibet), with the exceptions of Uyuni (Mg^{2+} - Na^+ signature) and the Northern Puna salars (Na^+ - K^+ signature). Brines with high Mg^{2+} concentrations occur in the Altiplano, whereas they are generally depleted in this cation in the Northern Puna. Finally, Ca^{2+} shows the highest concentrations in the Puna de Atacama, west of the modern Andean volcanic arc (Fig. 8).

The association between Li and B evidenced by our data (Figs. 6 c and d) confirms the existence of a link between these two chemical elements in Andean evaporitic systems, as was indicated by Catalano (1964), Alonso et al. (1988), Alonso et al. (1991), Kistler and Helvaci (1994), and observed in other parts of the globe (e.g., Helvaci et al., 2004, and references therein). However, isotopic studies have shown that, in the Andes, Li and B share only a partial common origin (Kaseman et al., 2004). Two distinctive origins have been suggested as sources for boron: for the western plateau, isotopic values indicate a volcanic contribution, mostly Neogene meso-silicic pyroclastic rocks and related hydrothermal systems, whereas weathering of volcanoclastic sequences from the Paleozoic basement are the probable source of B in the eastern plateau (Kaseman et al., 2004). The Paleozoic basement is also considered to be the primary source of Li (Egenhoff and Lucassen, 2003; Peralta Arnold et al., 2017; García et al., 2019; Meixner et al., 2019). Such common origin is reflected by the strong association between Li and B (R = 0.78; Fig. 6 d). However, their concentration ratios grading

up to 3:1, and the fact that they are mostly characterized by Li>B south of ~22°S and B>Li to the north of it, point to the absence of unambiguous Li:B patterns, consistently with B and Li being sourced from different lithologies. While it appears clear that further studies on the Li-B geochemical relationships are necessary (e.g., Lopez Steinmetz et al., 2020a), it seems safe to suggest that B may not be an appropriate prospective tool for lithium, at least not in the Andean region.

Despite that major brine chemistry, as discussed above, shows some degree of geographical organization with respect to compositions (Fig. 8), there is no obvious Li^+ distribution across the Andean plateau. Geographic patterns are also not observed for K, B, and Mg. The only common trend shown by those plots is that, as a whole, maximum Li^+ values were reported from salt pans located in the central area of the plateau, between 66°30' – 68°30' W and 20° – 24° S (Figs. 9 a and b). This spatial distribution is consistent with that of other cations, such as Mg^{2+} (Figs. 9 c and d), confirming that the most saline brines and highest ionic concentrations occur in the middle of the Andean plateau desert. It would thus be expected that solute concentrations would decrease in salt pans located towards the desert borders. This pattern is intriguing and clearly worthy of further studies. In summary, Li concentrations across the Andean plateau lack a clear geographic distribution pattern, other than that depicted in Figure 9.

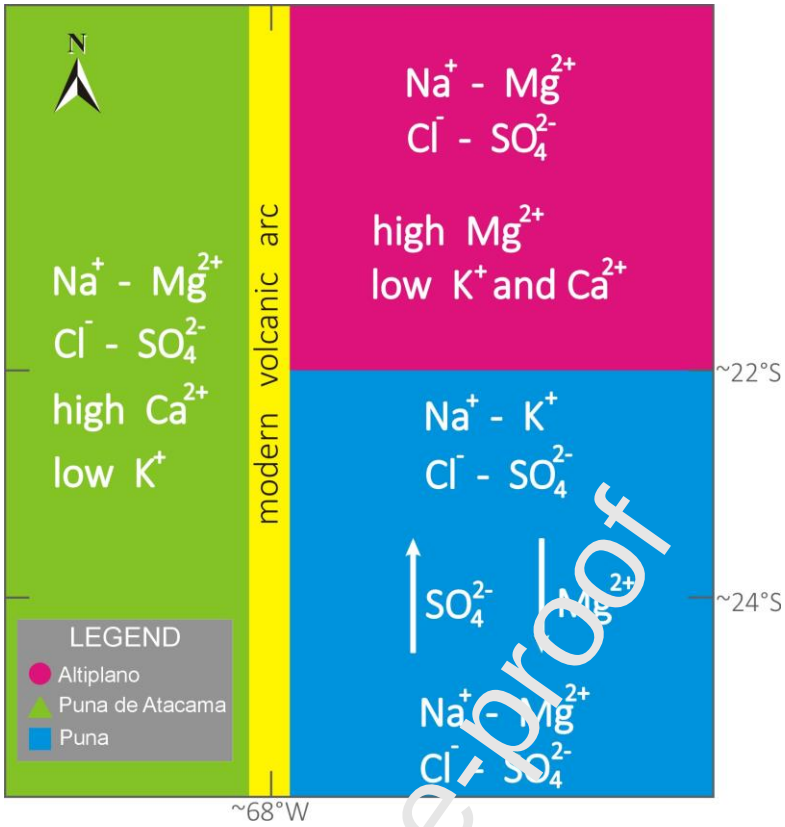

Figure 8. A schematic illustration of the internal subdivision of the Andean plateau (see legend), summarizing major brine chemistry in salt pans across the Lithium Crescent. "Modern volcanic arc" (yellow area) refers to the present-day situation; the past Cenozoic situation is not considered in this scheme.

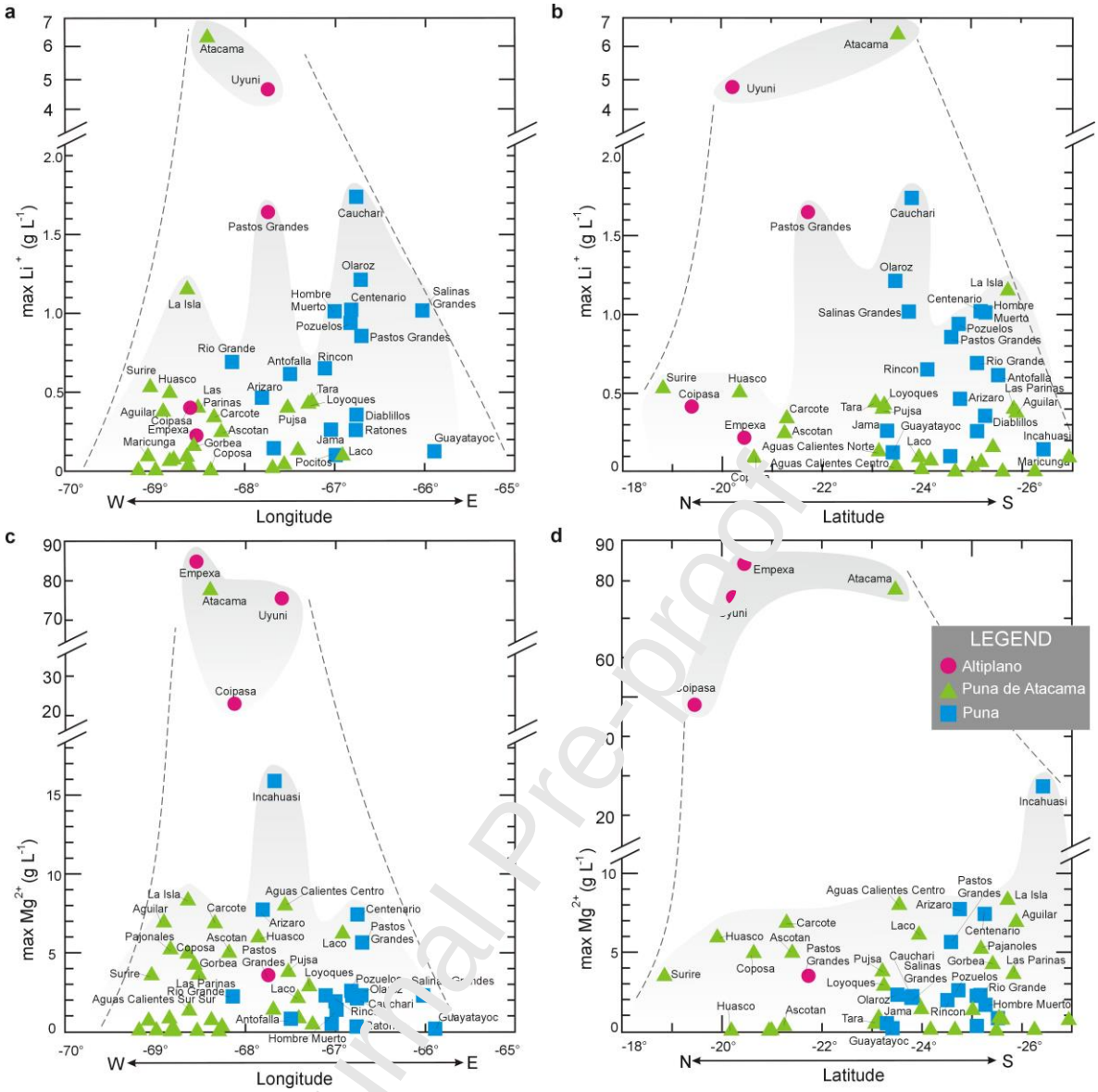

Figure 9. Scatter diagrams showing the maximum Li^+ (upper) and Mg^{2+} (bottom) concentrations according to longitude (a and c), and latitude (b and d) of salars across the Lithium Crescent. Notice that the considered maximum Li^+ and Mg^{2+} concentrations for Atacama are of 6,400 and 80,000 mg L^{-1}, respectively (Moraga et al., 1974; Ide and Kunasz, 1989; Kunasz, 2006). Plotted data correspond to values summarized in Table 4.

5.2. Link between salt pan and endorheic basin areas

The surfaces of the 55 salt pans studied across the Andean plateau (Fig. 1) appear to be related to those of their respective basin catchments, as revealed by the very good correlation obtained comparing their areas: R = 0.89 (Fig. 10 a). Two proportional size ranges are observed: basin catchments of Uyuni, Atacama and Arizaro are 5 times larger than their

salt pans, i.e., have a 1:5 size ratio (Fig. 10 a), whereas for the 52 remaining sites, salt pan to basin size proportions are close to the 1:10 ratio (Figs. 10 a and b). Coipasa and Guayatayoc are the two salt pans that least fit either of these relationships (these two cases are discussed further down).

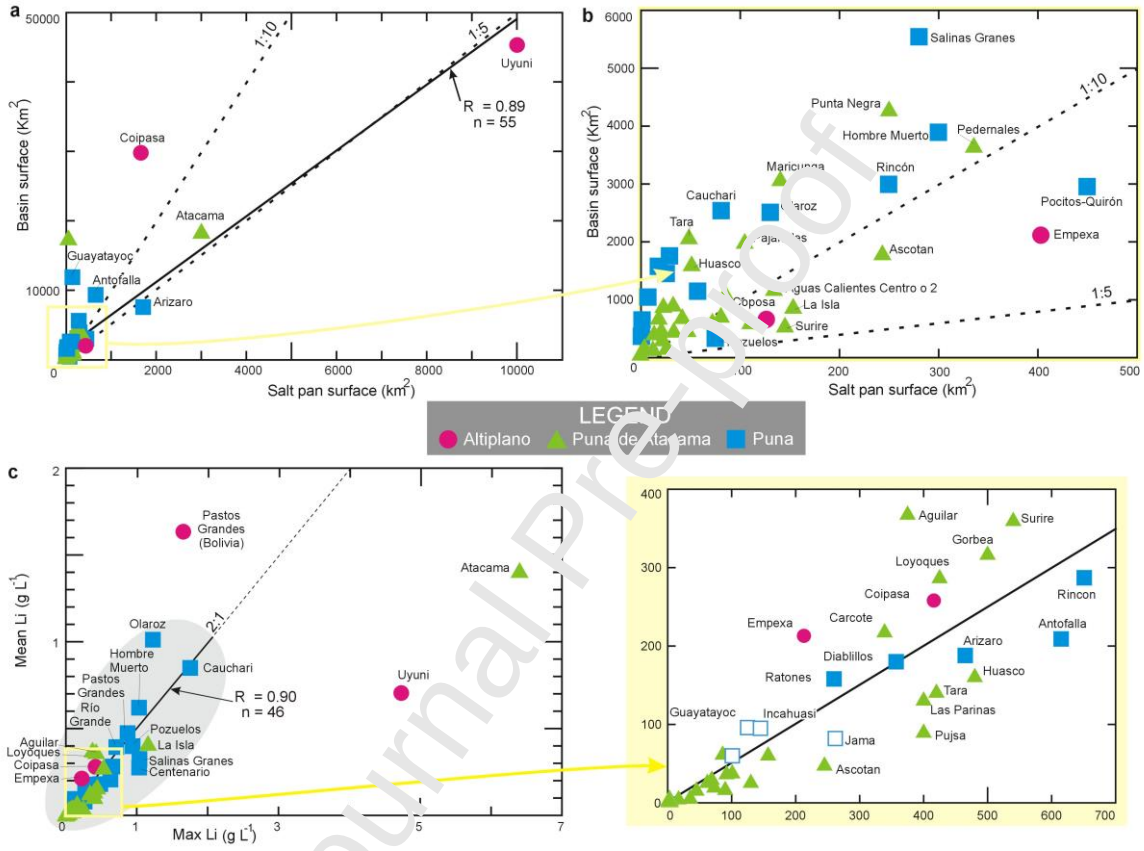

Figure 10. a and b) Scatter diagrams showing the relations between the surfaces of salt pans and their respective basin catchments. a) The correlation R = 0.89 was computed by considering all 55 Andean salt pans according to values summarized in Table 1. Note that the correlation line (continuous stroke) is close to the 1:5 proportion (dashed line). b) This panel expands the inset (in yellow) and plots data for the smallest salt pans. Note that most salt pans group close the 1:10 proportion. c) A scatter diagram plotting the relationship between the maximum (*Max*) and mean Li concentrations according to values summarized in Table 4. The regression R (continuous line) coincides with the stoichiometric proportion of 2:1 (dashed line) for 46 salt pans (n, gray area). Values for *max*/*mean Li* ratios are of 1 in Pastos Grandes (Bolivia), 7 in Uyuni, and 11 in Atacama. The inset offers an expanded view of the data displayed in the yellow box of panel c. R is the correlation coefficient (continuous lines), n is the number of salt pans.

The good correlation between salt pan and endorheic basin areas and the two proportional size ranges are very interesting patterns that undoubtedly deserve further specific investigation. Although this is beyond the purpose of this paper, it can be suggested that these relationships may arise from common trends in regional geological history, including lithology (i.e., substrate, tectonics, volcanism, etc.) and exogenous processes (e.g. climate-related such as regional aridity and its effect on rock weathering and erosion), across the Andean plateau.

Li-bearing Andean salt pans occur exclusively within endorheic basins. The onset of endorheism requires the convergence of the following parameters: suitable basin configuration (topographic barriers surrounding low lying areas), aridity (low precipitation – P – and high evaporation – E – rates, where P<E), hard substrate thus low erosion rates (in order for range-crossing rivers to fail incising deeply into the ranges and inhibit basin capture), and low aggradation rates (in order for sedimentation not to overfill the isolated area), amongst other variables (Sobel et al., 2003; Hilley and Strecker, 2005; García-Castellanos, 2006; Tremblay et al., 2015). Basement inherited heterogeneities (Hongn et al., 2007), Cenozoic Andean tectonics (actively uplifting ranges) and Neogene plateau rise were key factors for the formation of endorheic basins in the plateau, while the arid climate (Garreaud, 2009) has ensured their preservation (Vandervoort et al., 1995; López Steinmetz et al., 2020b). Within an endorheic basin, weathering and erosion of the catchments supply the suspended and dissolved load that is transported by rivers towards the low-laying area, where sediments and other products accumulate. Under arid conditions, salt pans form on these low-lying and hydrologically isolated areas (Melvin, 1991; Warren, 2010). Consequently, there is a clear link between the formation of internally drained areas and salt pans. However, as natural processes are typically heterogeneous and complex (Becker and Braun, 1999; Paola et al., 2009), this link clearly does not imply that we can estimate or model the size of endorheic

and saline units, let alone predict whether there might be proportionality between them. It could only be argued that if large catchments are more capable of generating a greater amount of suspended and dissolved load than smaller ones, then under similar conditions (i.e., geological history including lithology, deformation, volcanism and related hydrothermal processes, climate, etc.), large catchments would be required for the largest salt pans to form. For this reason, the fact that the size of salt pans adjusts proportionally to the size of endorheic basins, as revealed by our observations across the Andean plateau (Figs. 10 a and b), is a fascinating configuration for landscape studies. The salt pan/basin size proportionality could apply to other endorheic basins in arid regions. For instance, the Qaidam Basin (*ca*. 94°E - 38°N) in the northern Tibetan Plateau holds world-class Li-brine type deposits comprising 80% of the Li-brine resources found in China (Keslar et al., 2012). The basin's surface is 121,000 km^2, one-fourth of which covered by numerous saline lakes and playas (Yu et al., 2013). According to this, the ~1:4 salt pan/basin size ratio in Qaidam is close to the proportion found in Uyuni. The proportionality between the surfaces of salt pans and their endorheic basins should thus be checked in detail in other Tibetan Plateau basins and in other regions with internal drainage, in order to confirm the application of this relationship to other parts of the globe.

The poor salt pan-basin size association observed in the Guayatayoc and Coipasa salars appears to result from relatively late processes, i.e., younger than the basins. In the case of Guayatayoc, its basin is oversized with respect to the size of its salt pan (11,805 km^2 and 140 km^2, respectively). However, nearly half of the current extent of this basin formed in the Pleistocene, through the capture of the western watershed areas (López Steinmetz and Galli, 2015). This process resulted in the formation of a large (>500 km^2) distributive fluvial system (*sensu* Weissman et al., 2015), which lead to the subdivision of the precursor flats and the formation of two individual salars and respective basins, Salinas Grandes and Guayatayoc.

This means that, before the Pleistocene, the unified surface area of the basins (Salinas Grandes + Guayatayoc; ~11,000 km^2?) would correlate with the area of the precursor salt pans (Grandes + Guayatayoc + megafan, ~920 km^2?). In the case of Coipasa and its oversized basin area, satellite imagery of geomorphological features suggests that the northern half of the basin's catchments (north of 18°50'S) is a remnant of an ancient independent drainage system that could have been incorporated into the Coipasa basin through the capture of the Lauca River.

5.3. Mean Li concentrations are half the maximum Li measured

Brines in Andean salt pans show a 2:1 proportionality between maximum Li values and mean concentrations (Fig. 10 c), with a correlation R = 0.90 for 46 salt pans. Atacama, Uyuni and the Bolivian Pastos Grandes do not fit this correlation, with maximum to mean Li proportions of 11:1, 7:1, and 1:1, respectively. The high degree of correlation together with the exceptional number of salt pans fitting the 2:1 proportion make this pattern a substantial feature across the Central Andes. It means that maximum and mean Li concentrations can be considered as mutual proxies in surveying Li brine-type deposits. Accordingly, an indicative value of the mean concentration of Li brines in a salt pan can be estimated as half the value of the maximum measured, and vice versa, a relationship that can be expressed as:

$$\textit{mean}\ \text{Li} \approx ½\ \textit{max}\ \text{Li} \quad (1)$$

In the case where only few grade data were collected in one salt pan, the mean Li grade would be hard to determine. The difficulty in obtaining representative mean (and *max*) Li values arises from the need to acquire a large dataset in order for the mean Li (and *max*) grade to be confidently considered as representative of the real potentiality of the deposit in question (see Houston et al., 2011). However, despite the time elapsed since the beginning of the Andean Li rush, in general, the hydrochemistry of only a limited number of samples is

available for each of Andean salt pans in the scientific literature, even today. In fact, a relatively restricted number of data is also a typical situation in the initial phases of most mining projects. This clearly represents a major drawback when estimating the mean Li grades (and *max*) of mining prospects. In this context, the formulation (1) proposed for predicting average Li values can provide a useful approach. It is important to note that the *mean* Li value obtained through equation (1) is valid from a statistic and regional perspective. Obviously, it does not replace the specific average value of a deposit obtained from a large dataset, but provides a useful order-of-magnitude indication which that can be quite valuable (see for example the case of Salar de Olaroz in Fig. 10c and in Table 4, where *max* Li measured is of 1,213 mg L^{-1} whereas the average Li value that result from mining operations is of 841 mg L^{-1}; Garcia et al., 2019).

The usefulness of the formulation proposed above lies in the fact that at any point in the exploration of a Li brine-type deposit, the maximum measured Li concentration can be used to predict an indicative average value of its grade. The formulation (1) thus defines a dynamic approach to mean Li values, which implies that the predicted *mean* Li will change and evolve as the dataset increases during prospection.

5.4. Li grade as function of salt pan / basin geomorphology

As seen in previous sections, a regional assessment has made it possible to define a relationship between mean and maximum Li concentrations for Andean salars, and to identify a proportionality between the surfaces of the salt pans and basins. In order to test these proportionalities, the concentrations of Li, mean and maximum, have been addressed with respect to the area of the salt pan or its basin catchments (Fig. 11). Despite the fact that the link between Li concentrations and surfaces does not follow a definite proportionality, there is some degree of relationship between Li grade and salt pan size. Larger salt pans do host, by

and large, higher Li-grade brines than smaller pans (Fig. 11 a). This proportionality seems to change according to grade-size scales: i) a relationship of increasing Li with salt pan size is evident for the larger salt pans, i.e., more than 300 km^2 (R = 0.83, n = 7; Fig. 11 a); ii) this Li-grade/pan-surface relationship is also observed for salt pans having surfaces between 200 and 300 km^2 (R = 0.87, n = 4; Fig. 11, inset of panel a); and iii) a Li-grade/pan-surface relationship is also observed in those less than ~150 km^2 (R = 0.63, n = 23, Fig. 11 a, see also details in panels b and c). These three proportionality ranges comprise most (i.e., 34) of the Andean salt pans, with 15 salt pans not fitting any relationship (Fig. 11 b).

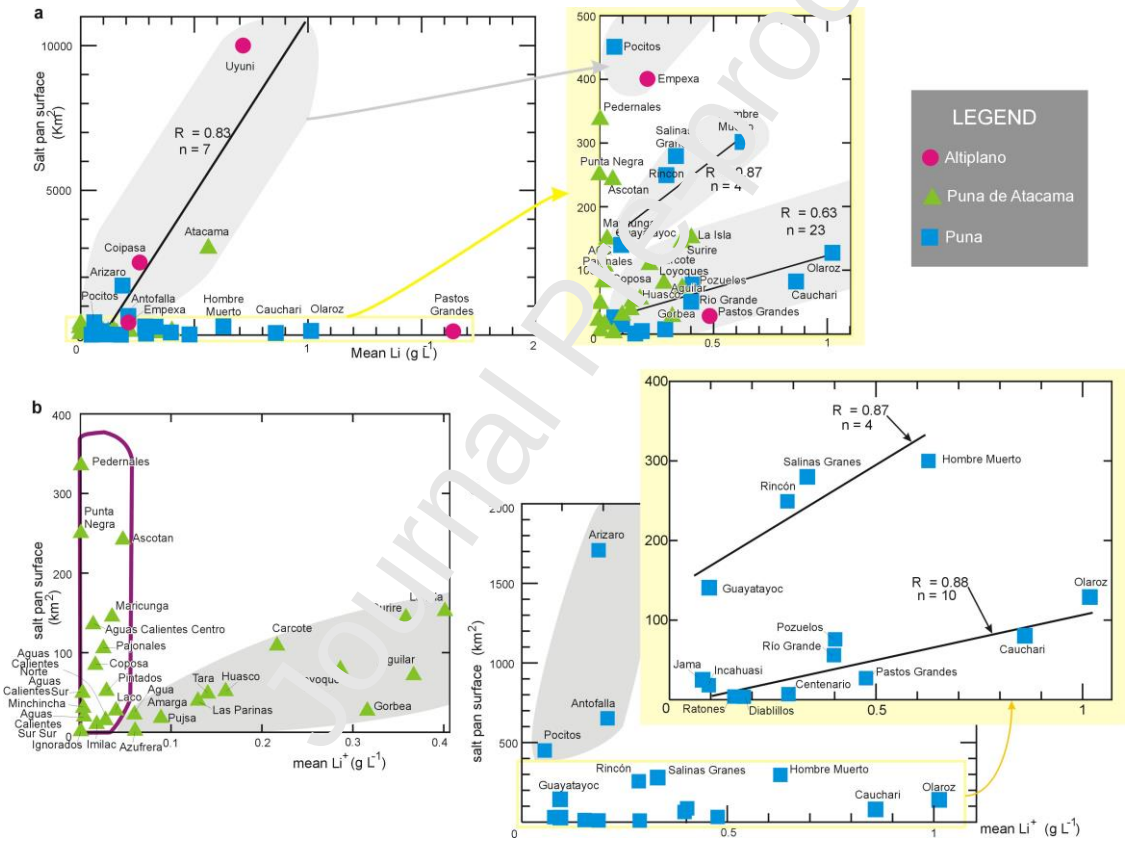

Figure 11. Scatter diagrams showing the relations between mean Li concentrations and pan surfaces for a) the 49 salt pans in the Andean plateau, b) salt pans from the Puna de Atacama, and c) salt pans from the Puna. Insets offer detailed views of the data displayed in the yellow boxes of panels a) and c). Gray areas group salt pans where there is some degree of proportionality between the mean Li values and the salt pans surfaces. In panel b, the purple thick line contours the 13 salt pans lacking a relationship between Li grade and salt pans surface. R is the correlation coefficient (continuous lines), n is the number of salt pans.

Arguably, the dependence of Li concentration on processes occurring at the basin scale is not the most widespread concept, particularly in the Andean and Tibetan literature. In most studies, the rate of supply of Li-bearing waters from hydrothermal springs is deemed as being the essential parameter in controlling Li grades (e.g., Davis et al., 1986; Ide and Kunasz, 1989; Kesler et al., 2012; Godfrey et al., 2013). However, as discussed in section 5.1, thanks to recent investigations on isotopic systematics, it is now apparent that the primary sources of Li in the Andes, including what is supplied by hydrothermal springs, are restricted varieties of lithologies of the Paleozoic basement that underlies the plateau (Egenhoff and Lucassen, 2003; Peralta Arnold et al., 2017; García et al., 2018; Meixner et al., 2019).

Likewise, not to be confused are the concepts of Li grades and Li reserves. Larger salt pans (i.e., of greater areal extent) do not necessarily contain greater Li reserves. This is because the total Li of a brine-type deposit (i.e., its reserves) is provided by the physical parameters of the aquifer (real size – i.e., horizontal areal extent plus thickness of the aquifer –, hydraulic conductivity, transmissivity, etc.), in addition to the actual Li grade in the brine.

Up to now, and contrarily to reserves, the sizes of salt pans or basins have not been related to Li levels, in the Andes or elsewhere, nor have they ever been considered as an integral condition for higher Li graded brines. However, regional data from the Andes show some degree of proportionality between Li concentrations and the surface area of basins and pans. This might imply that, under otherwise comparable conditions (i.e., substrate and surface lithology, characteristics and density of structures, number, density and hydrochemistry of hydrothermal sources, climate, etc.), large salt pans in endorheic basins would generally contain brines with a higher lithium content than smaller ones.

5.5. Lithium Crescent: when basin size matters

The most relevant factors governing Li grades in salt pans are the existence of input sources of Li, hydrological isolation, and aridity (Munk et al., 2016). Based on the general tendency of increasing Li concentrations with salt pan/basin sizes (Fig. 11), it follows that Li grades should be also (at least partially, in addition to the factors mentioned above) dependent on a geomorphological feature: the salt pan area (or its catchment area; Fig. 12). As discussed above, under analogous conditions (i.e., substrate and surface lithology, characteristic and density of displaying structures, number, density, and hydrochemical characteristics of springs, climate, etc.), larger salt pans should be expected to contain higher Li-graded brines than smaller ones, which would be a very useful criterion for surveying brine-type deposits. A correspondence between Li grades and salar sizes may reflect the importance of basin scale processes such as rock weathering, isolation, evaporation, and time (López Steinmetz et al., 2020b). This would be consistent with the model proposed for the formation of the Atacama's and Olaroz's brines, which took place in a near-surface setting through geochemical processes such as low-temperature weathering, evaporation, formation of transition-zone brines, and ultimately crystallization of halite to increase the concentration of Li in the brines (Munk et al., 2018; Franco et al., 2020). As already mentioned in section 5.1., other studies have reported Li isotopic data showing that volcanic and Paleozoic basement rocks represent the primary source for Li in the Andean plateau (Egenhoff and Lucassen, 2003; Peralta Arnold et al., 2017; García et al., 2019; Meixner et al., 2019). These models are consistent with the absence of a clear geographical distribution of Li in salars across the plateau, because Li is sourced from a lithological unit that is widespread the Paleozoic basement that underlies the salars across the plateau. On the other hand, the fact that Li levels increase with increasing salar size suggests that other processes are acting at the scale of the basin, and these are likely tied to geomorphology, and, presumably, the age of the basin. The implication of the latter would be that older basins had more time than younger ones to accumulate the products of

weathering and evaporation. Time dependence of Li grades implies a significant role of the age of endorheism onset, of the history of Li supply and of the persistence of arid conditions.

In summary, the integrity of the available regional data evidences some degree of correspondence between Li grades and salar sizes. This thus implies that not only the largest but also the oldest salars would be the ones expected to contain the largest Li resources. The fact that Li grade could be a function of salt pan/basin geomorphology may provide an insight on new approaches toward understanding the formation of Andean salars, and, more generally, brine-type deposits worldwide.

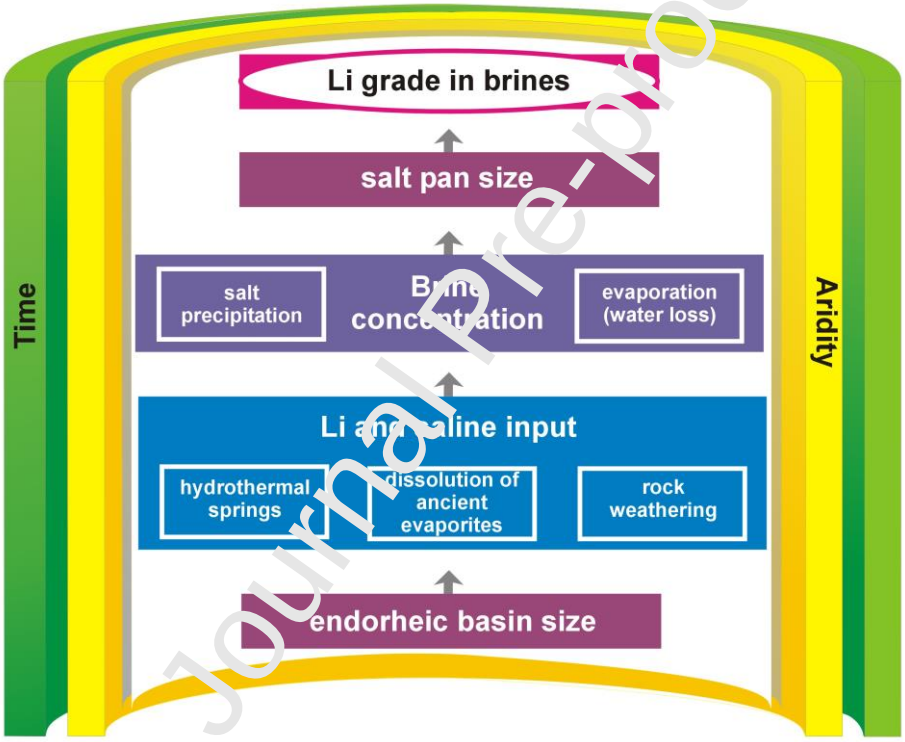

Figure 12. A schematic flow diagram illustrating Li -related processes from basin to salt pan (upwards). It illustrates the interplay between hydrological processes, climate and time, leading to Li accumulation (grade) in Andean brine-type deposits.

6. Conclusions

- The area involving all of the Andean Li-bearing salt pans extends beyond the Lithium Triangle and corresponds in fact to a curved crescent shape. We propose it be referred to as the Lithium Crescent.
- Andean brines are of the Cl^- - SO_4^{2-} type, and the compositional variability is marked by major cations: Na^+ - Mg^{2+} signatures largely predominate, with the exceptions of the Mg^{2+}>Na^+ signature of Uyuni, and the Na^+ - K^+ signature in the Northern Puna salars (Argentina). High Mg^{2+} concentrations occur in the Altiplano (Bolivia), and Ca^{2+} has highest values in the Puna de Atacama (Chile).
- Li lacks of a clear geographical distribution pattern across the Lithium Crescent, other than the fact that maximum Li^+ values occur in the central area of the Andean plateau, between 66°30' – 68°30' W and 20° – 24° S. Such an absence of a geographical distribution in the Li pattern is likely a consequence of the fact that the primary source of Li is the Paleozoic basement, which underlies all salt pans across the Andean plateau.
- Li-bearing Andean salt pans are exclusively hosted in endorheic basins. Across the Lithium Crescent, sizes of salt pans are proportionally related to the extent of their endorheic basin surface. The size ratio for the Qaidam Basin in the Tibetan Plateau is close to the proportions found at Uyuni. The salt pan/basin surface proportionality should thus be checked in detail in other regions of internal drainage, in order to confirm the application of this relationship to other parts of the globe.
- In the Andes, measured maximum Li values (max Li) are twice the mean Li concentrations: the equation *mean* Li ≈ ½ *max* Li can be employed to predict indicative mean grades during brine-type deposit surveying in the Lithium Crescent.
- The concentrations of Li (mean or maximum) can be addressed indistinctly with respect to the area of the salt pan or its basin catchments. Larger salt pans host, in general, higher-grade Li brines than smaller ones. This proportionality changes according to grade-size scales of

three groups: the largest salt pans of more than 300 km^2; those having surfaces between 200 and 300 km^2, and salt pans of less than ~150 km^2.

- Li levels depend on basin-scale processes, on geomorphology and, presumably, also on the age of the basin: therefore, it is likely the largest and oldest salars that are expected to hold the greatest Li concentrations.

ACKNOWLEDGMENTS

This research did not receive any specific grant from funding agencies in the public, commercial, or not-for-profit sectors. We wish to thank to C. Helvaci and five anonymous reviewers for their helpful comments that greatly improved this manuscript, as well as J.-A. Sanchez-Cabeza for editorial handling. The authors declare no conflict of competing financial nor non-financial interests in relation to the work herein.

Declaration of competing interests

The authors declare that they have no known competing financial interests or personal relationships that could have appeared to influence the work reported in this paper.

REFERENCES

Adad, M.J., López Steinmetz, R.L., Dávila, F.M., 2020. Seismic interpretation and Cenozoic tectonic evolution of the Pozuelos Basin, Andean Plateau, Argentina. Journal of South American Earth Sciences. doi:10.1016/j.jsames.2020.102938.

Allmendinger, R.W., Ramos, V.A., Jordan, T.E., Palma, M., Isacks, B.L., 1983. Paleogeography and Andean structural geometry, northwest Argentina. Tectonics. 2 (1), 1-16.

Allmendinger, R.W., Gubbels, T., 1996. Pure and simple shear plateau uplift, Altiplano-Puna, Argentina and Bolivia. Tectonophysics. 259 (1-3), 1-13.

Allmendinger, R., Jordan, T., Kay, S., Isacks, B., 1997. The evolution of the Altiplano–Puna plateau of the Central Andes. Annual Reviews on Earth and Planetary Sciences. 25, 139-174.

Alonso, H., Risacher, F., 1996. Geoquímica del Salar de Atacama, parte 1: origen de los componentes y balance salino. Revista Geológica de Chile. 23 (2), 113-122.

Alonso, R.N., Helvaci, C., Sureda, R.J., and Viramonte, J.G., 1988. A new Tertiary borax deposit in the Andes. Mineralium Deposita. 23, 299-305.

Alonso, R.N., Jordan, T.E., Tabbutt, K.T., Vandervoort, D.S., 1991. Giant evaporite belts of the Neogene Central Andes. Geology. 19, 401-404. doi:10.1130/0091-7613(1991)019<0401:GEBOTN>2.3.CO;2

Alonso, R.N., Bookhagen, B., Carrapa, B., Coutand, I., Haschke, M., Hilley, G.E., Schoenbohm, L., Sobel., E.R., Strecker, M.R., Trauth, M.H., Villanueva, A., 2006. Tectonics, climate, and landscape evolution of the southern central Andes: the Argentine Puna Plateau and adjacent regions between 22 and 30º S, in: Oncken, Chong, O., Franz, G., Giese, P., Götze, H.-J.. Ramos, V.A., Strecker, M.R., Wigger, P. (Eds.), The Andes Active Subduction Orogeny. Springer, Berlin, pp. 265-284.

An, J.W., Kang, D.J., Tran, K.T., Kim, M.J., Lim, T., Tran, T., 2012. Recovery of lithium from Uyuni salar brine. Hydrometallurgy. 64-70, 117-118.

Babeyko, Y.A., Sobolev, S.V., Trumbull, R.B., Oncken, O., Lavier, L.L., 2002. Numerical models of crustal scale convection and partial melting beneath the Altiplano-Puna plateau. Earth and Planetary Science Letters. 199, 373-388.

Baby, P., Rochat, P., Mascle, G., Herail, G., 1997. Neogene shortening contribution to crustal thickening in the back arc of the Central Andes. Geology. 25 (10), 883-886.

Belmonte, A., 2002. Krustale Seismizit7t, Struktur und Rheologie der Oberplatte zwischen der Pr7kordillere und dem magmatischen Bogen in Nordchile (228–248S). PhD thesis, Freie Universitat Berlin, Germany.

Banks, D., Markland, H., Smith, P.V., Mendez, C., Rodriguez, J., Huerta, A., Saether, O.M., 2004. Distribution, salinity and pH dependence of elements in surface waters of the catchment areas of the Salars of Coipasa and Uyuni, Bolivian Altiplano. J. of Geochem. Explor. 84, 141-166.

Becker, A., Braun, P., 199. Disaggregation, aggregation and spatial scaling in hydrological modelling. Journal of Hydrology. 217, 239-252.

Bevacqua, P.S.J., 1992. Geomorfología del Salar de Atacama y estratigrafía de su núcleo y delta, Segunda Región de Antofagasta, Chile. Undergraduate thesis (unpublished). Universidad Católica del Norte, Antofagasta, 284 p.

Borda, L.G., Franco, M.G., Córdoba, F., García, M.G., 2016. Geoquímica del Li y As en el salar de Olaroz, Puna de Jujuy. Resultados preliminares. 4th Reunión Argentina de Geoquímica de la Superficie (IV RAGSU). Actas de Resúmenes, 159.

Boschetti, T., Cortecci, G., Barbieri, M., Mussi, M., 2007. New and past geochemical data on fresh to brine waters of the Salar de Atacama and Andean Altiplano, northern Chile. Geofluids. 7, 33-50.

Bouttt, D.F., Hynek, S.A., Munk, L.A., Corenthal, L.G., 2016. Rapid recharge of fresh water to the halite-hosted brined aquifer of Salar de Atacama, Chile. Hydrological Processes. doi:10.1002/hyp.10994.

Brackebusch, L., 1883. Estudios sobre la Formación Petrolífera de Jujuy. Boletín de la Academia Nacional de Ciencias de Córdoba. 5, 137-252.

Brackebusch, L., 1891. Mapa geológico del interior de la República Argentina, escala 1:1.000.000. Gotha.

Canavan, R.R., Carrapa, B., Clementz, M.T., Quade, J., DeCelles, P., Schoenbohm, L.M., 2014. Early Cenozoic uplift of the Puna Plateau, Central Andes, based on stable isotope paleoaltimetry of hydrated volcanic glass. Geology. 42 (5), 447-450. doi:10.1130/G35239.1.

Catalano, L.R., 1964. Boro-Berilio-Litio (una nueva fuente natural de energía). Servicio Nacional Geológico Minero. Ministerio De Economía de la Nación Argentina, Buenos Aires, 99 p.

Carmona, V., Pueyo, J.J., Taberner, C., Chong, G., Thirlwall, M., 2000. Solute inputs in the Salar de Atacama (N. Chile). J. of Geochem. Explor. 69-70, 449-452.

Clark, F.W., 1924. The data of geochemistry, fifth ed. U.S. Geol. Survey Bull. 770, 841 p.

COCHILCO, 2013. Compilación de informes sobre Mercado internacional del litio y potencial del litio en salares del norte de Chile. Comisión Chilena del Cobre y SerNaGeoMin, Secretaría de Minería, Santiago de Chile, 319 p. http://www.cochilco.cl/estudios/info litio.asp.

Coira, B., Kay, S.M., Viramonte, J., 1993. Upper Cenozoic magmatic evolution of the Argentine Puna - A model for changing subduction geometry. International Geology Review. 35 (8), 677-720.

Corenthal, L.G., Boutt, D.F., Hynek, S.A., Munk, L.A., 2016. Regional groundwater flow and accumulation of a massive evaporate deposit at the margin of the Chilean Altiplano. Geophysical Research Letters. 43 (15), 8017-8025.

Crespo, P., Palma, H., Quintanilla, J., Quispe, L., 1987. Tratamiento químico de salmueras del Salar de Uyuni, Potosí. UMSa-ORSTOM, Informe 7.

Davis, J., Friedman, I., Gleason, J., 1986. Origin of the lithium-rich brine, Clayton Valley, Nevada. U.S. Geol. Surv. Bull. 1622, 131-138.

Dingman, R.J., 1967. Geology and ground-water resources of the northern part of the Salar de Atacama, Antofagasta Province, Chile. U.S. Geological Survey Bulletin. 1219.

Durán Iriza, R.J., 2012. Modelación numérica y su contribución al estudio del comportamiento hidrogeológico del sector SW del acuífero del Salar de Atacama, II Región de Antofagasta, Chile. Msc Thesis. Universidad de Chile, Facultad de Ciencias Físicas y Matemáticas, 201 p.

Egenhoff, S.O., Lucassen, F., 2003. Chemical and isotopic composition of lower to upper Ordovician sedimentary rocks (Central Andes /South Bolivia): implications for their source. Journal of Geology. 111, 487-497.

Ericksen, G.E., 1961. Rhyolite tuff, a source of the salts of northern Chile. Geol. Survey Research. U.S. Geological Survey Professional Paper. 424, C224-C225.

Ericksen, G.E., 1963. Geology of the salt deposits and the salt industry of northern Chile. U.S. Geological Survey. Open-File Report, 164 p.

Ericksen, G.E., Chong, G., Vila, T., 1976a. Lithium resources of salars in the central Andes. U.S. Geological Survey Professional Paper. 1005, 66-74.

Ericksen, G., Chong, G., Vila, T., 1976b. Lithium resources of salars in the central Andes, in: Vine, J.D., (Ed.), Lithium Resources and Requirements by the Year 2000. U.S. Geological Survey Professional Paper. 1005, 66-74.

Ericksen, G.E., Vine, J.D., Ballon, R., 1977. Lithium-rich brines at Salar de Uyuni and nearby salars in southwestern Bolivia. U.S. Geological Survey. Open-File Repository. 77-615, 52 p.

Ericksen, G.E., Salas, R., 1977. Geology and resources of salars in the central Andes. U.S. Geological Survey. Open File Repository. 88-210, 51 p.

Ericksen, G.E., Vine, J.D., Ballon, R.A., 1978. Chemical composition and distribution of lithium-rich brines in salar de Uyuni and nearby salars in southwestern Bolivia. Energy. 3 (3), 355-363.

Ericksen, G.E., Salas, R., 1987. Geology and resources of salars in the central Andes. U.S. Geological Survey. Open File Repository. 88-210, 51 p.

Eugster, H.P., 1980. Geochemistry of evaporitic lacustrine deposits. Ann. Rev. Earth Planet Sciences. 8, 35-63.

Franco, M.G., Borda, L., García, M.G., López Steinmetz, R.L., Flores, P., Córdoba, F., 2016. Geochemical and sedimentological characterization of the Salar de Olaroz, northern Argentinean Puna, Central Andes. 3rd International Workshop on Lithium, Industrial Minerals and Energy, Jujuy, Argentina.

Franco, M.G., Peralta Arnold, Y.J., Santamaría, C.D., López Steinmetz, R.L., Tassi, F., Venturi, S., Jofré, C.B., Caffe, P.J., Córdoba, F.E., 2020. Chemical and isotopic features of Li-rich brines from the Salar de Olaroz, Central Andes of NW Argentina, 2020. Journal of South American Earth Sciences. 103, 10742. doi:10.1016/j.jsames.2020.102742.

Garcés, I., López, P.L., Auqué, L.F., Chong, G., Vallès, V., Gimeno, M.J., 1996. Características geoquímicas generales del sistema salino del Salar de Llamara (Chile). Estudios Geológicos. 52, 23-35.

García, M.G., Borda, L.G., Godfrey, L.V., López Steinmetz, R.L., Losada Calderón, A., 2019. Characterization of lithium cycling in the Salar de Olaroz, Central Andes, using a geochemical and isotopic approach. Chemical Geology. 531, 119340. doi:10.1016/j.chemgeo.2019.119340.

García-Castellanos, D., 2006. Long-term evolution of tectonic lakes: Climatic controls on the development of internally drained basins, in: Willett, S.D., Hovius, N., Brandon, M.T., Fisher, D.M., (Eds.), Tectonics, Climate, and Landscape Evolution. Geological Society of

America Special Paper, 398. Penrose Conference Series, 283-294. doi:10.1130/2006.2398(17).

Garzione, C.N., Hoke, G.D., Libarkin, J.C., Withers, S., MacFadden, B., Eiler, J., Ghosh, P., Mulch, A., 2008. Rise of the Andes. Sciences. 320 (5881), 1304-1307. doi:10.1126/science.1148615.

Garzione, C.N., McQuarrie, N., Perez, N.D., Ehlers, T.A., Beck, S.L., Kar, N., Eichelberger, Chapman, A.D., Ward, K.M., Ducea, M.N., Lease, R.O., Poulsen, C.J., Wagner, L.S., Saylor, J.E., Zandt, G., Horton, B.K., 2017. Tectonic Evolution of the Central Andean Plateau and Implications for the Growthof Plateaus. Annual Review of Earth and Planetary Sciences. 45, 29-59.

Garreaud, R.D., 2009. The Andes climate and weather. Adv. in Geosci. 22, 3-11.

Garrett, D.E., 2004. Handbook of lithium and natural calcium chloride: their deposits, processing, uses and properties, fist ed. Elsevier Academic Press.

Gianni, G.M., Dávila, F., Echaurren, A., Fennell, L., Tobal, J., Navarrete, C.R., Quezada, P., Folguera, A., Giménez, M., 2018. A geodynamic model linking Cretaceous orogeny, arc migration, foreland basin subsidence and marine ingression in southern South America. Earth-Science Reviews 185, 437-462. doi:10.1016/j.earscirev.2018.06.016.

Godfrey, L.V., Chan, L. H., Alonso, R.N., Lowenstein, T.K., McDonough, W.F., Houston, J., Li, J., Bobst, A., Jordan, T.E., 2013. The role of climate in the accumulation of lithium-rich brine in the Central Andes. Applied Geochemistry. 38, 92-102.

Godfrey, L., Alvarez-Amado, F., 2020. Volcanic and saline lithium input to the Salar de Atacama. Minerals. 10, 201. doi:10.3390/min10020201.

Götze, H.-J., Krause, S., 2002. The Central Andean gravity high, a relic of an old subduction complex? Journal of South American Earth Sciences. 14, 799-811.

Gruber, P., Medina, P., 2010. Global lithium availability: a constraint for electric vehicles? Master thesis, University of Michigan, 76 p.

Hardie, L., Eugster, H., 1970. The evolution of closed-basin brines. Fiftieth Anniversary Symposia, Mineralogy and Geochemistry of Non-Marine Evaporites. Mineralogical Society of America Special Publication. 273-290.

Helvacı, C., Mordogan, H., Çolak, M., Gündogan, I, 2004, Presence and distribution of lithium in borate deposits and some recent lake waters of west-central Turkey. International Geology Review. 46, 177-190. doi:10.2747/0020-6814.46.2.177.

Herail, G., Oller, J., Baby, P., Bonhomme, M., Soler, P., 1993. Strike–slip faulting, thrusting and related basins in the Cenozoic evolution of the southern branch of the Bolivian Orocline. Tectonophysics. 259, 201-212.

Hilley, G.E., Strecker, M.R., 2005. Processes of oscillatory basin filling and excavation in a tectonically active orogen: Quebrada del Toro basin, NW Argentina. Geological Society of America Bulletin. 117, 887-901. doi:10.1130/B25602.1.

Hongn, F.D., Del Papa, C., Powell, J., Petrinovic, I., Mon, R., Deraco, V., 2007. Middle Eocene deformation and sedimentation in the Puna-Eastern Cordillera transition (23°-26°S): control by preexisting heterogeneities on the pattern of initial Andean shortening. Geology. 35, 271-274. doi:10.1130/G23189A.1.

Houston, J., Butcher, A., Ehren, P., Evans, K., Godfrey, L., 2011. The evaluation of brine prospects and the requirement for modifications to filing standards. Economic Geology. 106, 1225-1239.

Ide, F., Kunasz, I.A., 1989. Origin of lithium in Salar de Atacama, northern Chile, in: Ericken, G.E., Cañas Pinochet, M.T., Reinemund, J.A. (Eds.), Geology of the Andes and its relation to hydrocarbon and mineral resources. Circum-Pacific Council for Energy and Mineral Resources Earth Science Series, 11, pp. 165-172.

Isacks, B., 1988. Uplift of the Central Andean Plateau and bending of the Bolivian orocline. Journal of Geophysical Research: Solid Earth. 93, 3211-3231. doi:10.1029/JB093iB04p03211.

Jordan, T.E., Nester, P.L., Blanco, N., Hoke, G.D., Dávila, F., Tomlinson, A.J., 2010. Uplift of the Altiplano-Puna plateau: A view from the west. Tectonics. 29, TC5007. doi:10.1029/2010TC002661.

Kaseman, S.A., Meixner, A., Erzinger, J., Viramonte, J.G., Alonso, R.N., Franz, G., 2004. Boron isotope composition of the geothermal fluids and borate minerals from salar deposits (central Andes/NW Argentina). Journal of South American Earth Sciences. 16 (8), 685-697. doi:10.1016/j.jsames.2003.12.004.

Kay, S.M., Coira, B., Viramonte, J., 1994. Young mafic back arc volcanic rocks as indicators of continental lithospheric delamination beneath the Argentine Puna plateau, central Andes. Journal of Geophysical Research: Solid Earth. 99 (B12), 24323-24339.

Kesler, S.E., Gruber, P.W., Medina, P.A., Keoleian, G.A., Everson, M.P., Wallington, T.J., 2012. Global lithium resources: relative importance of pegmatites, brine and other deposits. Ore Geology Reviews. 48, 55-69.

Kistler, R.B., Helvacı, C., 1994. Boron and Borates. In: Carr DD (Ed.) Industrial Minerals and Rocks. Society of Mining, Metallurgy and Exploration. 6th Edition, 171-186.

Kunasz, I.A., 1976. Lithium resources - prospects for the future. In: Vine JD (Ed.) Lithium Resources and Requirements by the Year 2000. U.S. Geological Survey Professional Paper. 1005, 26-30.

Kunasz, I.A., 2006. Lithium resources, in: Kogel, J.E., Trivedi, N.C., Barker, J.M., Krukowski, S.T. (Eds.), Industrial minerals and rocks, commodities, markets and uses. Society for Mining, Metallurgy, and Exploration.

Langbein, W.B., 1961. Salinity and hydrology of closed lakes. U.S. Geological Survey Professional Paper. 412, 20 p.

Li, X., Mo, Y., Qing, W., Shao, S., Tang, C.Y., Li, J., 2019a. Membrane-based technologies for lithium recovery from water lithium resources: A review. Journal of Membrane Science. 591. doi:10.1016/j.memsci.2019.117317.

Li, Q., Fan, Q., Wang, J., Qin, J., Zhang, X., Wei, H., Du, Y., Shan, F., 2019b. Hydrochemistry, distribution and formation of lithium-rich brines in salt lakes on the Qinghai-Tibetan Plateau. Minerals. 9, 528. doi:10.3390/min9090528.

López, P.L., Auqué, L.F., Garcés, I., Chong, G., Vallès, V., Gimeno, M.J., 1996. Aplicaciones de la modelización geoquímica al estudio de pautas evolutivas en las salmueras del Salar de Llamara (Chile). Aproximación de método inverso. Estudios Geológicos. 52, 197-209.

López Julián, P.L., Garcés Millás, I.M., 2001. Relaciones geoquímicas entre los distintos tipos de aguas superficiales del salar de Surire (Chile). Departamento Ciencias de la Tierra, Universidad de Zaragoza, 10 p.

López Steinmetz, R.L., 2017. Lithium- and boron-bearing brines in the Central Andes: exploring hydrofacies on the eastern Puna plateau between 23° and 23°30'S. Mineralium Deposita. 52, 35-50.

López Steinmetz, R.L., Galli, C.I., 2015. Hydrological change during the Pleistocene-Holocene transition associated with the Last Glacial Maximum-Altithermal in the eastern border of northern Puna. Andean Geology. 42 (1), 1-19.

López Steinmetz, R.L., Fong, S.B., 2019. Water legislation in the context of lithium mining in Argentina. Resources Policy, 64, 101510. doi:10.1016/j.resourpol.2019.101510.

López Steinmetz, R.L., Montero-López, C., 2019. Stratigraphy and sedimentary environments of the Villa María and Peña Colorada formations (Paleogene), westernmost Argentine plateau. Latin American Journal of Sedimentology and Basin Analysis. 26 (1), 39-56.

López Steinmetz, R.L., Salvi, S., García, M.G., Béziat, D., Franco, G., Constantini, O., Córdoba, F., Caffe, P.J., 2018. Northern Puna plateau-scale survey of Li brine-type deposits in the Andes of NW Argentina. Journal of Geochemical Exploration. 190, 26-38.

López Steinmetz, R.L., Salvi, S., Sarchi, C., Santamans, C., López Steinmetz, L.C., 2020a. Lithium and brine geochemistry in the salars of the Southern Puna, Andean plateau of Argentina. Economic Geology. 115 (5), 1079-1096. doi:10.5382/econgeo.4754.

López Steinmetz, R.L., Avila, P., Dávila, F., 2020b. Landscape and drainage evolution during the Cenozoic in the Salinas Grandes Basin, Andean Plateau of NW Argentina. Geomorphology. 353, 107032. doi:10.1016/j.geomorph.2020.107032.

López Steinmetz, R.L., Avila, P., Dávila, F., 2020c. Landscape and drainage evolution during the Cenozoic in the Salinas Grandes Basin, Andean Plateau of NW Argentina. Geomorphology. 353, 107032. doi:10.1016/j.geomorph.2020.107032.

Lowenstein, T., Risacher, F., 2009. Closed basin brine evolution and the influence of Ca–Cl inflow waters. Death Valley and Bristol Dry Lake, California, Qaidam Basin, China, and Salar de Atacama, Chile. Aquat. Geochem. 15, 71-94.

Mardones, L., 1986. Caracteristicas geologicas e hidrogeologicas del Salar de Atacama. In Lagos, G. (Ed.), El litio: Un nuevo recurso para Chile. Universidad de Chile, Santiago, Chile, pp. 181-216.

Mardones, L., Chong, G., 1991. Consecuencias hidrológicas de la explotación del Salar de Atacama, Norte de Chile. 6th Congreso Geológico Chileno. Resúmenes expandidos, 719-722.

Maro, G., Caffe, P.J., Báez, W., 2017. Volcanismo monogenético máfico cenozoico de la Puna. 20th Congreso Geológico Argentino, Relatorio, 548-577.

McQuarrie, N., 2002. The kinematic history of the Central Andean fold-thrust belt, Bolivia: implications for building a high plateau. GSA Bulletin. 114 (8), 950-963.

Meixner, A., Sarchi, C., Lucassen, F., Becchio, R., Caffe, P.J., Lindsay, J., Rosner, M., Kasemann, S.A., 2019. Lithium concentrations and isotope signatures of Palaeozoic basement rocks and Cenozoic volcanic rocks from the Central Andean arc and back-arc. Mineralium Deposita. doi:10.1007/s00126-019-00915-2.

Melvin, J.L., 1991. Evaporites, Petroleum and Mineral Resources. Developments in Sedimentology, fiftieth ed. Elsevier, 556 p.

Mohr, S., Mudd, G., Giurco, D., 2010. Lithium Resources and Production: a critical global assessment. Prepared for CSIRO Minerals Down Under Flagship, by the Institute for Sustainable Futures, University of Technology, Sydney, and Department of Civil Engineering, Monash University. Final Report, 107 p.

Montero-López, C., Hongn, F., López Steinmetz, R.L., Aramayo, A., Pingel, H., Strecker, M.R., Cottle, J.M., Bianchi, C., 2020. Development of an incipient Paleogene topography between the present-day eastern andean plateau (Puna) and the Eastern Cordillera, southern Central Andes, NW Argentina. Basin Research. doi:10.1111/bre.12510.

Moraga, B.A., Chong, D.G., Fortt, M.A., Henriquez, A.H., 1974. Estudio geológico del Salar de Atacama, Provincia de Antofagasta. Instituto de Investigaciones Geológicas Boliviano. 29, 56 p.

Mpodozis, C., Ramos, V., 1989. The Andes of Chile and Argentina. In: Ericksen, G., Cañas-Pinochet, M., Reinemund, J. (Eds.), Geology of the Andes and its Relation to Hidrocarbon and Mineral Resources, Circum-Apcific Council for Energy and Mineral Resources Earth Sciences Series. 11, 59-90.

Munk, L.A., Hynek, S.A., Bradley, D., Boutt, D., Labay, K., Jochens, H., 2016. Lithium brines: A Global Perspective. Reviews in Economic Geology. 18, 339-365.

Munk, L.A., Boutt, D.F., Hynek, S.A., Moran, B.J., 2018. Hydrogeochemical fluxes and processes contributing to the formation of lithium-enriched brines in a hyper-arid continental basin. Chemical Geology. 493, 37-57.

Muñoz, N., Charrier, R., 1996. Uplift of the western border of the Altiplano on a west-vergent thrust system, northern Chile. Journal of South American Earth Sciences. 9, 171-181.

Orberger, B., Rojas, W., Millot, R., Flehoc, C., 2015. Stable isotopes (Li, O, H) combined with chemistry: powerful tracers for Li origins in Salar deposits from the Puna region, Argentina. Procedia Earth and Planetary Science. 13, 307-311.

Ovejero Toledo, A., Alonso, R.N., Ruiz, T., Quiroga, A.G., 2009. Evapofacies halítica en el Salar del Rincón, Departamento Los Andes, Salta. Revista de la Asociación Geológica Argentina. 64 (3), 493-500.

Paola, C., Kyle, S., Mohrig, D., Reinhardt, L., 2009. The "unreasonable effectiveness" of stratigraphic and geomorphic experiments. Earth-Science Reviews. 97, 1-43. doi:10.1016/j.earscirev.2009.05.003.

Peralta Arnold, Y.J., Cabssi, J., Tassi, F., Caffe, J.P., Vaselli, O., 2017. Fluid geochemistry of a deep-seated geothermal resource in the Puna plateau (Jujuy Province, Argentina). Journal of Volcanology and Geothermal Research. doi:10.1016/j.jvolgeores.2017.03.030.

Ramos, V., Cristallini, E., Pérez, D., 2002. The Pampean flat-slab of the Central Andes. Journal of South American Earth Sciences. 15, 59-78.

Rettig, S.L., Jones, B.F., Risacher, F., 1987. Geochemical evolution of brines in the Salar de Uyuni, Bolivia. Chemical Geology. 30, 57-79.

Riley, J.P., Tongudai, M., 1964. The lithium content of sea water. Deep Sea Research and Oceanographic Abstracts. 11 (4), 563-568. doi:10.1016/0011-7471(64)90002-6.

Risacher, F., Fritz, B., 1991. Quaternary geochemical evolution of the Salar of Uyuni and Coipasa, Central Altiplano, Bolivia. Chemical Geology. 90, 211-231.

Risacher, F., Alonso, H., 1996. Geoquímica del Salar de Atacama, parte 2: evolución de las aguas. Revista Geológica de Chile. 23 (2), 123-134.

Risacher, F., Alonso, H., Salazar, C., 1999. Geoquímica de aguas en cuencas cerradas: I, II y III Regiones – Chile. Convenio de Cooperación Dirección General de Aguas de Chile, Universidad Católica del Norte, Institut de Recherche pour le Developpement. Report 51, 781 p.

Risacher, F., Fritz, B., 2000. Bromine geochemistry of Salar de Uyuni and deeper salt crusts, Central Altiplano, Bolivia. Chemical Geology. 167, 373-392.

Risacher, F., Alonso, H., Salazar, C., 2002. Hydrochemistry of two adjacent saline lakes in the Andes of northern Chile. Chemical Geology. 187, 39-57.

Risacher, F., Alonso, H., Salazar, C., 2003. The origin of brines and salts in Chilean Salars: a hydrochemical review. Earth-Science Reviews. 63, 249-292.

Risacher, F., Fritz, B., 2009. Origin of salt and brine evolution of Bolivian and Chilean Salars. Aquat. Geochemistry. 15, 123-157.

Ruetenik, G.A., Hoke, G.D., Moucha, R., Val, P., 2018. Regional landscape response to thrust belt dynamics: The Iglesia basin, Argentina. Basin Research. 30. doi:10.1111/bre.12295.

Salas, J., Aravena, R., Guzmán, E., Comellà, O., Guimerà, J., Tore, C., Von Igel, W., Fock, A., Henríquez, A., 2009. Modelo de evolución hidroquímica e isotópica en el sistema de recarga del Salar de Atacama a través de su margen E. 12th Congreso Geológico Chileno, 1-4.

Scandiffio, G., Alvarez, M., 1990. Informe geoquímico sobre la zona geotérmica de Laguna Colorada, Bolivia. Geothermal investigations with isotope and geochemical techniques in Latin American. Proc. of a Final Res. Co-ordination Meeting, Organismo Internacional de Energía Atómica, Costa Rica, 77-113.

Scandiffio, G., Rodríguez, J., 1990. Geochemical report on the Sajama geothermal area, Bolivia. Geothermal investigations with isotope and geochemical techniques in Latin American. Proc of a Final Res Co-ordination Meeting, Organismo Internacional de Energía Atómica, Costa Rica, 114-168.

Schmidt, N., 2010. Hydrological and hydrochemical investigations at the Salar de Uyuni (Bolivia) with regard to the extraction of lithium. FOG. 26.

Schurr, B., Asch, G., Rietbrock, A., Kind, R., Pardo, M., Heit, B., Monfret, T., 1999. Seismicity and average velocities beneath the argentine Puna plateau. Geophysical Research Letters. 26 (19), 3025-3028.

Scott, E.M., Allen, M.B., Macpherson, C.G., McCaffrey, K.J.W., Davidson, J.P., Saville, C., Ducea, M.N., 2018. Andean surface uplift constrained by radiogenic isotopes of arc lavas. Nature Communications. 9, 969. doi:10.1038/s41467-018-03173-4.

Sempere, T., Butler, R.F., Richards, D.R., Marshall, L.G., Sharp, W. y Swisher, C.C. 1997. Stratigraphy and chronology of Upper Cretaceous-lower Paleogene strata in Bolivia and northwest Argentina. Bulletin of Geological Society of America. 109 (6), 709-727.

Sobel, E.R., Hilley, G.E., Strecker, M.R., 2003. Formation of internally drained contractional basins by aridity-limited bedrock incision. Journal of Geophysical Research. 108. doi:10.1029/2002JB001883.

Stoertz, G.E., Ericksen, G.E., 1974. Geology of salars in northern chile. U.S. Geological Survey Professional Paper. 811, 65 p.

Tassara, A., 2005. Interaction between the Nazca and South American plates and formation of the Altiplano–Puna plateau: Review of a flexural analysis along the Andean margin (15°-34°S). Tectonophysics. 399, 39-57. doi:10.1016/j.tecto.2004.12.014.

Teng, F.-Z., McDonough, W.F., Rudnick, R.L., Dalpé, C., Tomascak, P.B., Chapell, B.W., Gao, S., 2004. Lithium isotopic composition and concentration of the upper continental

crust. Geochimica et Cosmochimica Acta. 68 (20), 4167-4178. doi: 10.1016/j.gca.2004.03.031.

Tremblay, M.M., Fox, M., Schmidt, J.L., Tripathy-Lang, A., Wielicki, M.M., Harrison, T.M., Zeitler, P.K., Shuster, D.L., 2015. Erosion in southern Tibet shut down at ~10 Ma due to enhanced rock uplift within the Himalaya. Proceedings of the National Academy of Sciences of the United States of America. 112. doi: 10.1073/pnas.1515652112.

Turner, J.C., 1959. Estratigrafía del cordón de Escaya y de la Sierra de Rinconada (Jujuy). Revista de la Asociación Geológica Argentina. 13 (1-2), 15-39.

Vandervoort, D., Jordan, T., Zeitler, P., Alonso, R.N., 1995. Chronology of internal drainage development and uplift, southern Puna plateau, Argentina Central Andes. Geology. 23, 145-148. doi:10.1130/0091-7613(1995)023<0145:COIDDA>2.3.CO;2.

Vásquez, C., Ortíz, C., Suárez, F., Muñoz, J.F., 2013. Modeling flow and reactive transport to explain mineral zoning in the Atacama salt flat aquifer, Chile. Journal of Hydrology. 490, 114-125.

Vila, T., 1975. Geología de los depósitos salinos andinos, Provincia de Antofagasta, Chile. Revista Geológica de Chile. 2, 41-55.

Vinante, D., Alonso, R.N., 2006. Evapofacies del Salar del Hombre Muerto, Puna Argentina: distribución y génesis. Revista de la Asociación Geológica Argentina. 61 (2), 286-297.

Vine, J.D., 1976. Lithium Resources and Requirements by the Year 2000. U.S. Geological Survey Professional Paper. 1005, 169 p.

Warren, J.K., 2010. Evaporites through time: Tectonic, climatic and eustatic controls in marine and non-marine deposits. Earth-Science Reviews. 98, 217-268. doi:10.1016/j.earscirev.2009.11.004.

Weissman, G.S., Hartley, A.J., Scuderi, L.A., Nichols, G.J., Owen, A., Wright, S., Felicia, A.L., Holland, F., Anaya, F.M.L., 2015. Fluvial geomorphic elements in modern

sedimentary basins and their potential preservation in the rock record: A review. Geomorphology. 250, 187-219. doi:10.1016/j.geomorph.2015.09.005.

Whitman, D., Isacks, B.L., Kay, S.M., 1996. Lithospheric structure and along-strike segmentation of the Central Andean Plateau: seismic Q, magmatism, flexure, topography and tectonics. Tectonophysics. 259 (1-3), 29-40. doi:10.1016/0040-1951(95)00130-1.

Yu, J.Q., Gao, C.L., Cheng, A.Y., Liu, Y., Zhang, Y., He, X.H., 2013. Geomorphic, hydroclimatic and hydrothermal controls on the formation of lithium brine deposits in the Qaidam Basin, northern Tibetan Plateau, China. Ore Geology Reviews. 50, 171-183. doi:10.1016/j.oregeorev.2012.11.001.

Zheng, M., Liu, X., 2009. Hydrochemistry of Salt Lakes of the Qinghai-Tibet Plateau, China. Aquatic Geochemistry. 15, 293-320. doi:10.1007/s10498-008-9055-y.

Table 1. Altitude and comparative areal surfaces of Andean salt pans and of their endorheic basin catchments.

N° (Fig. 1)	Salt pan	Altitude (m asl)	Salt pan surface (km^2)	Basin surface (km^2)
1	Surire	4,260	144	574
2	Coipasa	3,656	1,650	29,817
3	Uyuni	3,633	10,000	45,239
4	Empexa	3,725	402	2,111
5	Huasco	3,778	51	1,572
6	Coposa	3,730	85	1,116
7	Michincha	4,130	25	282
8	Alconcha	4,250	4	128
9	Carcote	3,690	108	561
10	Ascotan	3,716	243	1,757
11	Pastos Grandes (Altiplano)	4,437	124	660
12	Atacama	2,300	3,000	18,100
13	El Tara	4,330	48	2,035

14	Aguas Calientes Norte o 1	4,280	15	281
15	Pujsa	4,500	18	634
16	Loyoques o Quisquiro	4,150	80	676
17	Aguas Calientes Centro o 2	4,200	134	1,168
18	El Laco	4,250	16	306
19	Aguas Calientes Sur o 3	3,950	46	476
20	Capur	3,950	27	137
21	Imilac	2,949	10	189
22	Punta Negra	2,945	250	4,253
23	Aguas Calientes Sur Sur o 4	3,665	20	656
24	Pajanoles	3,537	104	1,984
25	La Azufrera	3,580	3	214
26	Gorbea	3,950	27	324
27	Ignorados	4,250	1	38
28	Agua Amarga	3,55[illegible]	23	863
29	Aguilar	3,220	71	589
30	La Isla	[illegible],950	152	858
31	Los Infieles	3,520	7	293
32	Las Parinas	3,987	40	676
33	Salar Grande	3,950	29	867
34	Pedernales	3,370	335	3,620
35	Salar de la Laguna	3,494	1	400
36	La Piedra Parada	4,150	28	388
37	Wheelwright	4,220	6	466
38	Maricunga	3,760	145	3,045
39	Incahuasi	3,269	18	1,620
40	Antofalla-Botijuelas	3,330	655	9,259
41	Río Grande	3,668	56	1,155
42	Arizaro	3,474	1,708	7,508
43	Hombre Muerto	3,970	300	3,881
44	Diablillos	4,032	4	481
45	Ratones	3,822	3	605
46	Centenario	3,816	7	1,044
47	Pocitos-Quirón	3,663	450	2,969
48	Pozuelos	3,663	75	367
49	Pastos Grandes (Puna)	3,780	27	1,752

50	Rincón	3,725	250	3,017
51	Cauchari	3,903	80	2,557
52	Olaroz	3,903	130	2,519
53	Jama	4,080	25	1,500
54	Salinas Granes	3,410	280	5,529
55	Guayatayoc	3,400	140	11,805

Table 2. Chemical composition of brines from Andean salt pans. Hydrochemical data of the Altiplano salars correspond to values reported by Risacher and Fritz (1991), excepting for samples Uyu0, C0, EMP, and PGB that are from Ericksen and Salas (1987). Summarized data for the Puna de Atacama salars follow Risacher et al. (1999; summarized by COCHILCO, 2013), excepting for samples LAC0, SUR0, HCO0, ASC0, ATA0, ATAdo, and AZU0 that are from Ericksen and Salas (1987). Brine chemistry of the Puna salt pans follows data reported by López Steinmetz (2017), López Steinmetz et al. (2018), and López Steinmetz et al. (2020a), excepting for samples CE0, HM0, PG0, AR0, PC0, RI0, and RG0 that are from Ericksen and Salas (1987). TDS in g L^{-1}, remaining concentrations in mg L^{-1}.

	g L^{-1}	mg L^{-1}								
UYUNI										
sample	TDS	Ca	Mg	Na	K	Li	Cl	SO4	CO3	HCO3	B
uyu0	351	461	11,800	94,900	13,500	700	191,800	13,200	-	592	1,136
UA15	121	545	7,780	107,000	9,380	412	190,000	9,550	-	-	302
UA80	122	310	16,100	91,800	17,600	770	190,000	23,000	-	-	669
UA200	123	316	16,600	90,300	17,300	812	191,000	22,400	-	-	655
UA400	123	327	16,800	94,900	17,400	812	196,000	22,500	-	-	657
UA600	123	315	17,300	91,400	17,600	826	192,000	24,400	-	-	668
UB10	125	137	38,400	57,000	29,700	1,780	200,000	43,900	-	-	1,710
UB100	224	149	51,000	36,100	19,400	2,560	210,000	32,800	-	-	2,020
UB250	125	50	55,400	28,800	19,400	2,790	214,000	34,300	-	-	2,160
UB400	125	50	55,900	29,200	19,700	2,830	215,000	34,600	-	-	2,190

UC5	123	233	32,300	68,300	20,100	1,460	194,000	30,700	-	-	1,230
UC100	122	268	19,200	88,600	19,000	888	190,000	25,600	-	-	843
UC250	122	269	19,300	88,600	18,600	868	192,000	26,200	-	-	871
UC400	122	269	19,200	89,200	18,800	881	191,000	26,700	-	-	970
UD10	122	208	30,600	66,200	26,700	1,310	197,000	30,800	-	-	1,240
UD100	122	317	19,900	85,100	21,600	888	194,000	22,600	-	-	864
UD250	122	293	19,200	87,600	20,300	819	193,000	25,300	-	-	864
UD400	122	294	19,300	88,100	20,300	819	191,000	25,400	-	-	871
UE5	123	294	24,500	78,700	22,600	708	195,000	27,700	-	-	987
UE100	122	269	17,600	92,000	19,300	708	190,000	29,400	-	-	871
UE250	122	269	17,400	92,200	19,300	708	190,000	28,600	-	-	859
UE400	122	269	17,300	92,000	19,300	708	189,000	28,100	-	-	860
UF30	121	654	7,390	109,000	7,430	339	190,000	10,300	-	-	239
UF110	121	618	7,630	108,000	7,510	339	190,000	10,700	-	-	232
UG15	121	834	5,780	112,000	5,790	254	190,000	8,200	-	-	171
UG95	121	738	6,390	110,000	6,180	266	191,000	9,140	-	-	199
UG270	121	666	6,970	109,000	6,800	303	190,000	9,790	-	-	233
UH10	121	760	6,930	109,000	7,190	315	191,000	8,960	-	-	236
UH100	121	666	7,850	107,000	7,940	351	190,000	10,100	-	-	266
UH300	122	437	11,500	100,000	10,300	463	189,000	18,700	-	-	372
UH500	122	401	12,100	98,200	10,500	488	189,000	20,300	-	-	397
UH700	122	391	12,100	99,400	10,800	489	190,000	20,700	-	-	405
UH900	122	367	12,600	100,000	11,200	513	188,000	22,200	-	-	423
UI15	121	714	6,660	109,000	7,120	303	190,000	9,370	-	-	226
UI100	121	702	6,630	106,000	6,760	303	189,000	9,360	-	-	214
UI1000	121	569	7,290	106,000	7,590	303	189,000	14,100	-	-	261
UJ15	121	786	7,000	107,000	7,590	339	190,000	8,930	-	-	254
UJ100	122	521	11,1	100,0	11,00	584	191,0	14,20	-	-	399

			00	00	0		00	0			
UJ300	122	437	12,800	95,900	12,000	560	189,000	18,100	-	-	437
UJ700	122	391	14,100	94,800	12,400	575	187,000	24,100	-	-	525
UK10	122	622	8,820	103,000	8,880	413	191,000	11,000	-	-	288
UK100	122	417	14,700	94,300	14,600	685	192,000	18,700	-	-	457
UK200	123	319	15,600	93,800	14,400	688	190,000	25,100	-	-	453
UK400	123	295	15,900	93,800	24,000	688	187,000	28,500	-	-	441
UL20	122	401	17,500	87,600	19,500	805	194,000	16,000	-	-	452
UL100	122	390	17,100	87,900	17,800	805	195,000	16,300	-	-	557
UL250	122	340	18,900	82,800	17,400	840	190,000	18,100	-	-	590
UM17	121	638	6,420	109,000	7,160	277	189,000	7,870	-	-	669
UM100	122	425	13,500	91,000	12,000	559	191,000	15,100	-	-	319
UM400	122	269	16,300	92,500	13,900	672	187,000	26,000	-	-	461
UN16	122	354	19,100	85,600	18,000	868	194,000	19,100	-	-	563
UN100	122	354	19,400	85,100	19,400	916	193,000	19,300	-	-	591
UN300	123	245	21,700	80,500	19,400	979	192,000	24,800	-	-	718
UO9	121	533	10,500	103,000	10,800	471	191,000	11,600	-	-	250
UO100	122	342	17,800	89,200	16,600	784	190,000	20,000	-	-	533
UO500	123	234	21,800	88,600	18,300	937	190,000	36,000	-	-	892
UP17	122	378	16,700	82,600	16,300	756	192,000	17,100	-	-	486
UP100	122	305	20,600	78,200	19,400	930	193,000	21,000	-	-	662
UP500	123	282	21,300	77,300	19,000	944	193,000	24,000	-	-	770
UQ17	120	577	7,290	111,000	7,510	313	190,000	9,020	-	-	141
UQ100	121	533	9,400	104,000	9,460	399	190,000	10,900	-	-	232
UQ450	121	545	9,960	101,000	9,660	411	192,000	11,700	-	-	241
UQ800	121	509	10,400	98,200	10,000	424	190,000	12,800	-	-	202
UR15	121	457	5,690	112,000	5,470	217	190,000	8,090	-	-	639
UR100	121	565	8,090	107,000	7,980	314	190,000	10,800	-	-	101

UR450	121	577	8,310	106,000	8,330	338	188,000	11,200	-	-	134
UR800	122	413	12,500	102,000	11,300	413	187,000	19,700	-	-	482
US9	120	577	6,340	108,000	6,650	276	190,000	8,870	-	-	164
US100	121	606	7,630	106,000	7,980	314	192,000	10,500	-	-	195
US450	122	401	11,200	99,400	12,000	389	187,000	21,600	-	-	494
US00	122	294	13,500	101,000	14,000	465	186,000	30,300	-	-	785
UT15	121	642	6,830	109,000	7,470	278	190,000	10,100	-	-	198
UT100	120	626	6,970	107,000	7,350	277	189,000	10,200	-	-	197
UT450	121	630	6,900	106,000	7,230	260	190,000	10,200	-	-	195
UT800	121	533	8,310	106,000	8,800	327	189,000	13,000	-	-	244
UU20	121	565	10,300	106,000	6,660	350	188,000	12,300	-	-	273
UU350	120	533	8,970	103,000	7,590	291	191,000	11,800	-	-	275
UU700	121	388	10,800	107,000	8,580	316	188,000	19,200	-	-	328
UV10	121	630	8,140	110,000	6,450	242	191,000	10,100	-	-	235
UV100	121	618	8,020	110,000	6,490	242	190,000	10,600	-	-	244
UV500	121	618	8,020	108,000	6,370	242	191,000	10,700	-	-	226
UW22	123	380	27,700	69,900	22,800	1,030	200,000	18,800	-	-	1,080
UW100	123	463	20,900	86,300	16,200	784	196,000	14,200	-	-	878
UX90	123	294	28,900	72,000	17,700	1,130	195,000	22,600	-	-	1,060
UX300	123	307	28,900	72,000	17,900	1,180	195,000	23,000	-	-	1,050
UY16	121	726	7,190	111,000	6,330	254	191,000	8,690	-	-	238
UY100	121	581	9,550	105,000	8,130	340	190,000	11,100	-	-	315
UY300	122	354	14,500	97,800	12,600	500	189,000	22,200	-	-	650
UY600	122	316	15,300	96,400	13,100	511	188,000	24,800	-	-	712
UZ12	121	557	8,890	101,000	9,190	484	191,000	9,890	-	-	303
UZ100	122	413	15,100	95,700	12,400	536	191,000	16,300	-	-	557
UZ450	122	354	17,100	92,900	13,400	599	192,000	19,300	-	-	608
UZ800	122	342	17,0	91,10	13,30	598	190,0	19,50	-	-	665

			00	0	0		00	0			
U112	122	425	16,600	92,000	15,800	701	196,000	17,000	-	-	578
U1400	123	264	21,300	86,500	19,200	895	197,000	29,500	-	-	987
U1800	123	247	21,600	83,700	19,500	930	193,000	31,700	-	-	1,040
U213	121	433	14,500	92,900	14,300	640	195,000	15,900	-	-	480
U2100	122	331	17,300	92,000	16,600	750	196,000	23,000	-	-	618
U2200	122	307	17,700	88,300	17,400	791	193,000	25,200	-	-	700
U2300	122	284	18,700	86,500	17,900	826	190,000	27,400	-	-	766
U2400	123	234	20,400	85,600	18,600	909	187,000	33,100	-	-	976
U2500	123	223	20,500	85,600	18,600	916	189,000	34,100	-	-	1,010
U2600	123	223	20,700	85,600	18,400	895	187,000	34,100	-	-	1,020
YA17	121	577	9,530	102,000	12,200	435	192,000	10,100	-	-	360
YA100	121	449	12,200	95,900	13,600	557	191,000	13,700	-	-	483
YB11	120	758	4,370	111,000	4,690	144	190,000	5,830	-	-	155
YB100	121	581	8,650	103,000	8,910	338	190,000	10,200	-	-	299
YB500	121	364	11,100	93,200	12,900	534	189,000	19,800	-	-	488
YC12	120	662	3,840	112,000	3,860	120	191,000	5,070	-	-	103
YC100	120	638	6,660	107,000	6,450	229	189,000	8,540	-	-	219
YD9	120	758	6,030	107,000	6,450	229	191,000	7,470	-	-	216
YD100	121	421	12,200	94,800	12,500	496	192,000	14,400	-	-	427
YD450	120	341	15,500	90,200	14,500	621	191,000	20,200	-	-	615
YD800	122	329	16,500	90,200	15,400	670	192,000	22,700	-	-	692
YE8	121	662	5,300	110,000	5,750	193	192,000	6,300	-	-	204
YE100	121	400	12,400	95,900	12,600	509	192,000	15,200	-	-	438
YE450	125	274	17,200	91,500	16,100	673	195,000	28,100	-	-	790
YE800	123	269	16,900	89,500	15,800	661	191,000	27,400	-	-	791
YF23	120	1,030	2,960	113,000	3,090	72	192,000	4,690	-	-	88
YF200	120	854	4,500	109,000	4,650	144	190,000	6,240	-	-	143

YG15	121	473	11,000	100,000	10,600	521	191,000	12,000	-	-	301
YG100	120	806	4,520	112,000	5,160	228	191,000	6,020	-	-	164
YH1	126	100	51,000	37,300	26,800	2,460	207,000	44,400	-	-	2,030
YH100	125	137	53,200	34,000	19,900	2,590	212,000	29,200	-	-	1,950
YH250	125	87	53,900	32,400	19,900	2,590	213,000	29,500	-	-	2,040
YI8	121	517	8,410	105,000	8,800	362	192,000	9,030	-	-	273
YI100	121	533	9,330	101,000	9,310	399	192,000	9,590	-	-	305
YI450	121	509	9,840	100,000	9,930	411	191,000	10,100	-	-	321
YI800	121	437	11,000	95,400	11,000	484	191,000	11,500	-	-	351
YJ17	120	698	6,660	110,000	8,640	301	193,000	8,110	-	-	271
YJ100	121	461	11,800	94,100	12,700	545	194,000	12,800	-	-	428
YJ400	122	257	16,900	88,800	16,100	743	189,000	27,200	-	-	620
YK1	120	710	7,780	105,000	8,210	325	191,000	10,400	-	-	277
YK100	121	529	9,870	101,000	10,200	410	192,000	11,700	-	-	320
YK400	122	304	15,100	93,600	13,900	584	190,000	24,000	-	-	522
YK700	122	281	16,400	97,500	15,300	634	189,000	27,000	-	-	576
YL22	120	794	4,370	112,000	4,930	156	192,000	6,250	-	-	141
YL100	121	455	9,380	102,000	9,580	375	193,000	12,800	-	-	324
YL400	121	421	10,400	100,000	10,500	423	191,000	14,800	-	-	360
RA130	101	429	197	1,550	80	10	3,380	600	-	-	21
RB180	102	1,200	566	6,650	300	27	12,500	2,400	-	-	31
RC120	105	846	3,400	19,600	1,800	14	40,100	5,700	-	-	116
RD160	109	1,950	4,670	39,800	3,200	217	79,500	5,120	-	-	250
RE100	114	2,670	8,650	61,600	6,140	575	129,000	3,600	-	-	481
RF90	115	1,660	9,430	65,100	7,310	631	135,000	5,700	-	-	837
RG30	116	1,250	11,400	69,200	7,900	674	147,000	7,650	-	-	546
RH10	121	565	10,200	97,500	10,500	538	190,000	11,100	-	-	368
RI15	120	457	13,500	81,900	12,400	736	171,000	15,600	-	-	507

RJ10	122	390	11,400	95,700	11,000	633	190,000	12,800	-	-	626
RK90	115	1,930	10,500	62,600	7,820	701	137,000	5,100	-	-	1,020
RL110	111	2,530	6,440	45,500	5,000	417	96,600	4,830	-	-	971
RM100	109	2,130	5,780	37,000	4,500	347	80,200	5,100	-	-	318
RN75	115	2,020	3,890	79,100	4,500	359	132,000	5,000	-	-	491
RO80	114	1,590	6,730	62,600	5,400	483	122,000	7,200	-	-	965
RP50	110	1,960	2,330	45,500	2,800	182	82,000	6,990	-	-	137
RQ70	113	1,320	5,270	62,600	4,500	272	110,000	9,700	-	-	507
RR60	116	1,240	4,130	88,100	4,500	239	145,000	7,250	-	-	419
RS15	127	52	69,000	12,500	17,600	4,230	231,000	31,400	-	-	3,700
RT15	127	60	68,800	14,000	17,600	4,930	229,000	29,500	-	-	3,520
RU1	124	238	27,200	66,200	26,400	1,600	198,000	30,900	-	-	1,420
RV20	122	413	13,400	101,000	11,700	563	189,000	13,900	-	-	507
RW10	122	338	15,100	97,500	15,700	763	191,000	19,800	-	-	623
RX10	127	69	61,000	21,300	19,100	3,550	223,000	32,000	-	-	3,450
RY95	116	1,840	11,700	63,000	6,840	763	138,000	6,100	-	-	766
RZ1	128	102	75,300	10,700	15,100	4,720	253,000	26,500	-	-	4,330
CA0	124	315	10,900	105,000	9,230	237	185,000	28,100	-	-	720

COIPASA

sample	TDS	Ca	Mg	Na	K	Li	Cl	SO4	CO3	HCO3	B
C0	368	253	12,120	100,400	9,080	338	186,000	25,300	-	785	2,208
CA150	124	194	14,100	104,000	10,000	275	172,000	54,000	-	-	870
CA250	126	164	10,500	111,000	8,330	212	132,000	104,000	-	-	644
CB0	123	301	10,700	108,000	9,190	237	187,000	29,300	-	-	690
CB150	126	102	23,000	94,700	14,300	416	168,000	80,100	-	-	1,350
C10	121	541	10,200	104,000	7,120	198	189,000	14,700	-	-	601
C20	122	521	15,100	99,100	11,600	333	188,000	17,600	-	-	952
C3	122	319	10,1	109,0	7,310	205	179,0	25,90	-	-	614

			00	00			00	0			
C40	122	509	10,800	107,000	8,560	230	187,000	18,000	-	-	640
C50	121	738	6,800	111,000	5,980	154	186,000	13,900	-	-	428
EMPEXA											
sample	TDS	Ca	Mg	Na	K	Li	Cl	SO4	CO3	HCO3	B
EMP	239	259	8,480	67,200	3,400	213	120,000	34,100	-	430	702
PASTOS GRANDES (ALTIPLANO)											
sample	TDS	Ca	Mg	Na	K	Li	Cl	SO4	CO3	HCO3	B
PGB	321	3,100	3,480	101,000	14,200	1,64[illegible]	[illegible]4,000	2,460	-	-	3041
EL TARA											
sample	TDS	Ca	Mg	Na	K	Li	Cl	SO4	CO3	HCO3	B
TAR-RT-001	1	108	12	340	7	4	596	46	19	83	18
TAR-RT-002	1	96	10	350	7	4	612	47	0	135	19
TAR-RT-003	1	88	8	275	6	3	478	35	6	91	15
TAR-RT-004	2	92	14	525	18	6	846	68	0	157	17
TAR-RT-005	1	80	20	440	8	4	688	66	0	141	11
TAR-RT-006	1	80	20	415	12	4	680	64	0	137	11
TAR-RT-007	90	300	435	56,000	580	420	87,400	6,060	0	2,350	710
TAR-RT-008	79	275	350	48,000	420	340	69,800	7,480	0	1,981	570
TAR-RT-009	16	100	208	7,100	480	34	10,740	1,036	52	1,689	119
TAR-RT-010	2	84	32	600	40	6	836	159	62	333	16
TAR-RT-011	112	1,450	430	80,000	700	440	127,000	11,240	0	1,102	486
TAR-RT-012	103	1,400	440	76,000	640	420	123,200	10,700	0	1,060	415
AGUAS CALIENTES NORTE											
sample	TDS	Ca	Mg	Na	K	Li	Cl	SO4	CO3	HCO3	B
ACN-RT-001	1	94	24	340	8	4	602	58	0	154	8
ACN-RT-002	1	94	26	225	7	3	480	55	0	160	6
ACN-RT-003	1	86	22	330	12	4	578	62	8	98	5
ACN-RT-004	3	240	12	1,100	18	6	2,100	101	0	50	9
ACN-RT-005	12	800	50	4,300	56	20	8,260	270	0	209	28
ACN-RT-006	5	320	100	1,600	34	10	2,930	229	0	452	16
ACN-RT-007	50	2,800	820	23,000	1,020	130	40,800	3,010	0	842	392
PUJSA											
sample	TDS	Ca	Mg	Na	K	Li	Cl	SO4	CO3	HCO3	B

PUJ-RT-001	-	125	35	280	28	2	338	384	0	173	0
PUJ-RT-002	-	180	790	26,000	2,825	175	37,000	15,000	834	1,324	450
PUJ-RT-003	-	180	835	32,000	3,175	200	39,800	22,600	1,016	1,477	529
PUJ-RT-004	-	70	28	260	26	1	286	264	0	225	0
PUJ-RT-005	-	50	12	220	16	1	232	208	0	128	0
PUJ-RT-006	-	175	250	23,000	975	60	12,880	32,200	586	0	177
PUJ-RT-007	-	300	98	9,500	300	20	3,520	15,440	457	0	184
PUJ-RT-008	-	80	16	1,050	32	2	441	1,600	52	186	0
PUJ-RT-009	-	1,000	1,515	52,000	3,400	400	87,200	14,340	0	1,542	317
PUJ-RT-010	-	525	183	13,000	525	27	5,[illegible]00	21,960	548	568	230
LOYOQUES											
sample	TDS	Ca	Mg	Na	K	Li	Cl	SO4	CO3	HCO3	B
LOY-RT-001	3	220	34	890	[illegible]2	6	1,765	97	40	0	4
LOY-RT-002	123	18,000	2,300	9,600	123	350	202,000	1,820	0	655	430
LOY-RT-003	123	15,850	2,475	100,[illegible]00	123	375	196,800	1,720	0	779	681
LOY-RT-004	122	17,600	2,855	[illegible]6,000	128	425	194,800	1,840	0	827	756
LOY-RT-005	102	5600	2,135	[illegible]2,000	1,650	275	114,200	2,600	0	733	527
AGUAS CALIENTES CENTRO											
sample	TDS	Ca	Mg	Na	K	Li	Cl	SO4	CO3	HCO3	B
ACC-RT-001	15	[illegible]2,425	415	3,750	325	10	10,740	1,302	0	143	0
ACC-RT-002	7	600	413	2,150	228	5	4,660	752	0	448	0
ACC-RT-003	11	1,650	273	2,600	240	8	7,260	882	0	142	0
ACC-RT-004	44	875	3,338	19,000	1,025	45	33,800	5,530	0	819	33
ACC-RT-005	9	575	293	2,800	150	8	5,840	236	0	144	0
EL LACO											
sample	TDS	Ca	Mg	Na	K	Li	Cl	SO4	CO3	HCO3	B
LAC0	210	820	6,251	62,200	4,800	101	109,630	15,360	-	620	1,078
LAC-RT-001	44	1,300	2,035	19,000	1,525	40	34,200	5,370	0	400	0
LAC-RT-002	47	1,225	2,645	21,000	1,850	33	36,300	7,280	0	428	0
LAC-RT-003	43	800	2,165	19,000	1,550	28	32,200	5,930	0	370	0
LAC-RT-004	26	775	1,10	12,00	900	20	18,08	3,768	0	367	0

			2	0			0				
LAC-RT-005	2	190	34	650	95	2	1,090	340	0	175	0
AGUAS CALIENTES SUR											
sample	TDS	Ca	Mg	Na	K	Li	Cl	SO4	CO3	HCO3	B
ACT-RT-001	33	1,625	1,370	13,000	900	18	24,360	4,160	0	225	0
ACT-RT-002	6	275	170	2,100	182	3	3,590	642	0	81	0
ACT-RT-003	2	180	62	500	60	1	980	447	0	109	0
ACT-RT-004	2	170	60	550	60	1	935	424	0	104	0
ACT-RT-005	7	425	193	2,400	155	3	4,170	606	0	353	0
ACT-RT-006	1	410	33	250	27	1	256	1,186	0	57	0
ACT-RT-007	4	230	150	1,100	85	5	1,850	689	0	243	0
ACT-RT-008	2	140	85	650	46	3	1,135	343	0	164	0
AGUAS CALIENTES SUR SUR											
sample	TDS	Ca	Mg	Na	K	Li	Cl	SO4	CO3	HCO3	B
ACS-RT-001	1	85	43	400	40	1	590	332	0	92	1
ACS-RT-002	1	85	43	375	39	1	594	334	0	93	1
ACS-RT-003	1	85	43	400	40	2	590	330	0	96	2
ACS-RT-004	25	750	850	10,300	1,050	35	18,400	4,060	66	349	131
ACS-RT-005	1	100	16	175	4	<1	194	334	0	42	0
ACS-RT-006	1	100	16	175	3	<1	193	344	0	42	0
ACS-RT-007	1	83	16	175	3	<1	197	342	0	41	0
ACS-RT-008	3	190	100	875	100	3	1,380	1,010	0	111	9
ACS-RT-009	3	170	86	750	80	2	1,115	895	0	99	7
ACS-RT-010	7	375	98	3,050	270	9	3,930	2,160	0	117	40
PAJONALES											
sample	TDS	Ca	Mg	Na	K	Li	Cl	SO4	CO3	HCO3	B
PAJ-RT-001	16	775	500	6,500	325	6	11,580	1,084	0	76	36
PAJ-RT-002	15	775	475	5,800	305	6	10,740	894	0	74	31
PAJ-RT-003	1	625	250	5,000	285	5	8,940	1,042	0	75	27
PAJ-RT-004	36	2,125	1,175	1,360	925	16	28,450	2,850	0	190	85
PAJ-RT-005	35	1,900	1,150	15,000	900	16	27,500	2,685	0	182	91
PAJ-RT-006	39	2,375	1,275	13,800	1,025	18	29,300	3,100	0	208	102
PAJ-RT-007	67	2,525	1,975	33,400	1,725	58	62,000	2,550	0	314	177
PAJ-RT-008	71	2,625	2,175	33,800	1,825	62	67,400	2,820	0	448	190
PAJ-RT-009	48	1,300	1,525	2,050	1,275	40	40,400	1,650	0	334	125
PAJ-RT-010	78	5,700	2,300	33,800	1,675	31	76,800	590	0	193	86

PAJ-RT-011	54	4,945	2,275	20,100	1,208	18	47,600	780	0	134	54
PAJ-RT-012	47	4,635	2,025	16,600	1,135	18	39,300	0	0	135	46
PAJ-RT-013	68	5,018	1,750	30,800	1,803	35	61,300	3,700	0	511	329
PAJ-RT-014	69	5,018	1,800	32,000	1,828	35	62,200	3,730	0	523	349
PAJ-RT-015	69	5,018	1,775	31,700	1,810	35	63,400	3,720	0	516	334
PAJ-RT-016	96	5,018	3,050	52,800	2,800	45	104,000	200	0	864	524
PAJ-RT-017	96	5,015	3,275	53,400	2,825	44	102,400	2,820	0	854	457
PAJ-RT-018	84	5,018	2,400	4,120	2,315	41	82,400	3,380	0	704	402
PAJ-RT-019	19	1,540	375	6,100	353	8	13,900	725	0	46	54
PAJ-RT-020	19	1,542	375	6,300	345	8	13,350	705	0	46	54
PAJ-RT-021	23	2,065	475	7,500	405	9	17,100	865	0	52	58
PAJ-RT-022	23	1,915	450	7,600	410	9	16,400	1,055	0	60	59
PAJ-RT-023	24	1,980	500	7,800	430	10	17,450	1,155	0	64	64
PAJ-RT-024	23	1,900	475	7,800	405	10	17,000	1,085	0	63	62
PAJ-RT-025	103	9,500	5200	50,800	2,200	36	118,800	2,060	0	399	195

GORBEA

sample	TDS	Ca	Mg	Na	K	Li	Cl	SO4	CO3	HCO3	B
GOR-RT-001	66	163	39,500	66,000	5,000	475	162,806	107,367	0	0	2,084
GOR-RT-002	66	165	38,500	64,000	4,600	500	156,595	102,355	0	0	1,986
GOR-RT-003	76	410	27,500	52,000	5,000	300	124,711	74,825	0	0	1,509
GOR-RT-004	76	275	28,000	52,000	5,000	300	123,753	74,290	0	0	1,458
GOR-RT-005	5	425	550	1,300	25	5	2,486	3,107	0	0	4,559

AGUA AMARGA

sample	TDS	Ca	Mg	Na	K	Li	Cl	SO4	CO3	HCO3	B
AAM-RT-001	15	2363	325	3,600	185	14	10,540	1,308	0	112	69
AAM-RT-002	15	2448	300	3,700	198	14	10,650	1,150	0	113	69
AAM-RT-003	109	23,000	3,525	51,200	1,980	58	136,000	1,120	0	166	397
AAM-RT-004	113	25,000	4,225	59,400	2,035	61	150,000	1,200	0	162	426

AAM-RT-005	105	23,000	3,000	47,600	1,683	56	124,400	1,120	0	170	392
AMA-04	93	24,100	3,090	43,200	2,490	157	121,000	674	0	0	515
LA ISLA											
sample	TDS	Ca	Mg	Na	K	Li	Cl	SO4	CO3	HCO3	B
LIS-RT-001	5	150	78	2,000	42	13	3,167	666	0	32	0
LIS-RT-002	30	350	450	13,000	880	98	22,661	2,118	0	73	10
LIS-RT-003	8	165	125	3,000	75	23	4,839	857	0	41	0
LIS-RT-004	13	475	183	5,200	275	30	8,650	1,201	0	35	0
LIS-RT-005	15	375	250	6,200	375	35	9,928	1,273	0	42	0
LIS-RT-006	23	425	25	9,600	750	73	16,200	1,624	0	50	0
LIS-RT-007	123	525	5,300	12,000	8,600	850	189,388	14,292	0	188	272
LIS-RT-008	123	500	5,000	130,000	800	800	196,701	13,687	0	152	268
LIS-RT-009	123	475	4,900	126,000	800	800	180,054	13,362	0	152	262
LIS-RT-010	122	525	5,400	122,000	8,600	875	191,338	14,864	0	190	297
LIS-RT-011	120	525	8,300	110,000	108,000	1,150	189,057	17,884	0	1,173	284
LIS-RT-012	45	195	925	21,000	1,575	78	35,351	2,346	44	132	26
AGUILAR											
sample	TDS	Ca	Mg	Na	K	Li	Cl	SO4	CO3	HCO3	B
AGU-RT-001	113	55,000	6,800	60,000	2,600	375	212,126	1,382	0	860	692
AGU-RT-002	113	55,000	6,900	60,000	2,600	375	206,750	0	0	862	697
AGU-RT-003	115	45,000	6,100	62,000	2,600	350	191,125	0	0	1,029	829
LAS PARINAS											
sample	TDS	Ca	Mg	Na	K	Li	Cl	SO4	CO3	HCO3	B
LPA-RT-001	9	105	95	4,100	54	10	6,058	498	0	211	14
LPA-RT-002	7	100	65	2,600	41	7	4,431	341	0	209	6
LPA-RT-003	7	113	75	3,300	44	8	4,786	368	0	217	0
LPA-RT-004	7	130	73	2,900	45	7	4,672	480	0	87	0
LPA-RT-005	122	725	3,200	100,000	500	350	170,111	12,796	0	580	423
LPA-RT-006	123	625	3,600	105,000	6,000	400	167,584	12,522	0	651	447
SURIRE											
sample	TDS	Ca	Mg	Na	K	Li	Cl	SO4	CO3	HCO3	B
SUR0	236	890	3,830	73,200	13,200	540	131,380	11,430	-	-	3,700

SUR-22	12	1,160	84	1,710	310	8	1,800	4,060	26	297	544
SUR-23	285	850	2,960	93,400	14,100	530	155,000	11,500	0	0	1,300
PEDERNALES											
sample	TDS	Ca	Mg	Na	K	Li	Cl	SO4	CO3	HCO3	B
PED-26	1	135	43	711	50	3	1,250	305	1	127	9
PED-27	1	125	42	711	48	3	1,180	341	8	126	9
PED-28	2	166	58	817	61	3	1,450	387	1	92	10
PED-29	1	145	46	699	51	3	1,260	334	0	103	10
MARICUNGA											
sample	TDS	Ca	Mg	Na	K	Li	Cl	SO4	CO3	HCO3	B
MAR-16	4	165	58	1,220	161	11	3,200	169	0	273	18
MAR-17	2	147	17	543	63	5	927	175	0	227	11
MAR-19	51	1,240	680	16,200	1,230	92	30,800	171	0	0	50
PINTADOS											
sample	TDS	Ca	Mg	Na	K	Li	Cl	SO4	CO3	HCO3	B
PIN-07	68	4,530	0	19,300	2,510	69	39,800	1,900	0	0	21
PIN-16	1	43	9	435	49	1	689	121	1	9	10
PIN-41	23	529	179	7,080	696	15	5,890	58	11	124	60
HUASCO											
sample	TDS	Ca	Mg	Na	K	Li	Cl	SO4	CO3	HCO3	B
HCO0	277	610	5,680	65,000	13,500	480	112,980	26,700	-	-	2,333
HCO-6	0	11	8	122	13	<1	82	74	1	2	2
HCO-9	0	13	5	45	11	<1	20	156	0	59	1
COPOSA											
sample	TDS	Ca	Mg	Na	K	Li	Cl	SO4	CO3	HCO3	B
COP- 03	0	7	4	14	3	<1	10	38	0	9	1
COP-07	3	214	163	573	45	2	1,010	488	2	79	4
COP-08	0	32	18	29	6	<1	28	67	0	146	1
COP-09	3	362	53	483	50	1	753	1,030	1	111	3
COP-11	112	742	4,930	31,100	3,080	90	50,800	20,400	16	465	101
COP-16	2	119	44	382	18	1	742	235	1	63	2
MICHINCHA											
sample	TDS	Ca	Mg	Na	K	Li	Cl	SO4	CO3	HCO3	B
MIC-08	0	25	19	35	18	<1	18	-	0	90	<1
MIC-09	0	32	8	41	16	<1	25	-	2	46	<1
MIC-10	1	69	25	33	12	<1	24	-	0	25	<1
MIC-11	0	10	3	15	7	<1	10	-	0	31	<1

MIC-13	0	20	12	15	6	<1	14	-	0	37	<1
ALCONCHA											
sample	TDS	Ca	Mg	Na	K	Li	Cl	SO4	CO3	HCO3	B
ALC-01	1	150	2	97	13	<1	90	-	0	87	3
CARCOTE											
sample	TDS	Ca	Mg	Na	K	Li	Cl	SO4	CO3	HCO3	B
CAR-04	176	12,000	1,990	49,500	2,880	136	107,000	1,280	6	134	426
CAR-09	2	88	32	593	53	2	1,130	35	0	66	5
CAR-16	322	2,810	6,850	101,000	12,500	339	19,500	2,440	0	0	0
CAR-19	20	678	352	5,680	712	4	4,690	2,320	5	136	66
ASCOTAN											
sample	TDS	Ca	Mg	Na	K	Li	Cl	SO4	CO3	HCO3	B
ASC0	154	920	5,125	45,000	3,530	186	70,000	25,000	-	2,900	2,520
ASC-01	3	111	22	679	190	8	1,160	179	0	225	40
ASC-02	1	58	29	192	26	1	315	105	1	211	3
ASC-03	0	85	21	524	76	6	898	120	0	204	30
ASC-04	2	131	31	570	65	5	1,080	191	1	67	7
ASC-15	2	87	22	536	77	6	888	124	0	200	30
ASC-16	0	19	4	96	15	1	107	63	0	90	4
ASC-17	5	205	143	1,110	113	5	1,680	672	3	714	58
ASC-41	118	1,170	2,410	35,400	4,890	245	58,600	12,200	40	958	1,030
ASC-47	3	15	37	860	96	4	1,080	194	80	365	21
ATACAMA											
sample	TDS	Ca	Mg	Na	K	Li	Cl	SO4	CO3	HCO3	B
ATA0	870	520	6,130	103,000	12,900	760	193,100	16,140	-	560	1,705
ATAdo	385	300	8,500	98,000	19,500	1,200	182,800	25,500	-	220	1,673
ATA	370	450	9,650	91,100	23,600	1,570	189,500	15,900	-	230	440
Do1	310	1,100	6,350	85,800	13,000	940	163,900	8,540	0	280	360
Do2	190	900	5,330	45,100	9,000	520	83,780	18,170	0	240	360
Do3	73	360	1,810	18,220	4,220	290	36,750	3,430	0	320	100
Do4	62	1,080	1,930	14,840	2,900	190	27,500	7,900	0	100	88
Do5	40	1,060	750	10,280	1,690	130	20,300	2,160	0	92	61
ATA-05	2	136	60	520	50	4	959	271	1	254	20
ATA-22	4	151	128	1,070	196	13	1,880	552	1	429	13
IMILAC											

sample	TDS	Ca	Mg	Na	K	Li	Cl	SO4	CO3	HCO3	B
IMI-01	1	39	3	132	11	<1	96	233	1	28	2
IMI-03	6	593	52	1,460	73	73	1,970	1,900	0	68	6
IMI-04	2	11	7	30,400	19	1	1,000	60	13	73	2
IMI-8D	12	642	66	3,800	94	2	6,430	1,010	0	66	8
PUNTA NEGRA											
sample	TDS	Ca	Mg	Na	K	Li	Cl	SO4	CO3	HCO3	B
PUN-08	7	78	24	2,420	140	3	3,980	101	1	70	2
PUN-16	3	9	53	653	89	3	1,560	420	0	40	20
PUN-18	3	158	24	791	104	2	1,440	240	0	6	10
PUN-19	1	19	3	127	15	<1	172	30	5	79	1
PUN-20	1	3	0	175	8	<1	132	37	30	129	0
PUN-24	0	31	2	139	9	<1	244	37	1	13	0
IGNORADOS											
sample	TDS	Ca	Mg	Na	K	Li	Cl	SO4	CO3	HCO3	B
IGN-04	10	485	445	342	342	1	444	6,490	0	0	18
IGN-05	13	505	707	637	637	2	1,410	7,300	0	0	29
LA AZUFRERA											
sample	TDS	Ca	Mg	Na	K	Li	Cl	SO4	CO3	HCO3	B
AZU0	400	88	48,640	69,000	14,960	86	172,130	87,990	-	0	740
AZU-07	1	117	9	34	11	<1	157	148	0	29	0
JAMA											
sample	TDS	Ca	Mg	Na	K	Li	Cl	SO4	CO3	HCO3	B
JA1	7	1,780	402	2,004	201	6	2,560	7,009	0	349	539
JA2	7	991	243	2,860	343	11	2,627	4,587	0	387	3,070
JA3	6	131	17	3,523	210	10	6,170	2,051	0	332	236
JA4	6	122	48	3,422	344	2	4,927	2,537	0	234	493
JA5	6	65	47	4,183	297	2	5,868	1,219	0	263	239
JA6	91	647	469	60,432	4,591	262	97,017	14,615	0	286	1,421
JA7	6	122	48	3,475	344	2	4,929	2,535	0	341	493
JA8	6	122	47	3,482	344	2	4,930	2,541	0	344	494
JA9	90	647	467	60,427	3,356	262	97,018	14,616	0	282	1,421
JA10	92	646	492	60,437	4,658	261	97,017	14,616	0	272	1,422
OLAROZ											
sample	TDS	Ca	Mg	Na	K	Li	Cl	SO4	CO3	HCO3	B
OL1	157	584	1,539	112,191	5,051	771	181,749	9,678	0	421	2,090

OL2	158	529	1,981	112,190	5,504	968	181,003	10,222	0	419	2,090
OL3	155	526	1,972	107,654	6,019	1,007	179,627	10,192	0	435	2,302
OL4	157	481	2,301	107,956	7,984	1,207	180,837	8,982	0	328	3,176
OL5	137	448	2,183	69,855	6,563	1,092	175,695	10,585	0	343	2,511
OL6	153	496	2,276	79,670	7,870	1,213	187,041	10,015	0	366	2,251
OL7	158	513	1,988	107,759	5,179	868	176,345	9,856	0	331	2,422
OL8	160	537	2,186	107,069	5,501	1,093	184,987	10,203	0	280	3,037
OL9	159	447	1,628	112,332	6,003	1,061	179,091	10,658	0	247	2,800
OL10	145	598	1,970	71,783	6,569	861	181,605	10,374	0	266	2,655
CAUCHARI											
sample	TDS	Ca	Mg	Na	K	Li	Cl	SO4	CO3	HCO3	B
CA1	97	556	1,851	69,826	2,976	535	108,014	9,060	0	279	1,337
CA2	92	764	1,509	58,032	2,714	442	102,211	14,471	0	355	2,190
CA3	124	603	1,676	83,709	8,594	1,740	130,406	11,958	0	490	2,834
CA4	139	477	1,594	101,347	4,769	713	149,818	16,356	0	461	2,304
CA5	144	599	2,110	104,515	4,733	873	163,886	9,685	0	623	2,126
SALINAS GRANDES											
sample	TDS	Ca	Mg	Na	K	Li	Cl	SO4	CO3	HCO3	B
SG1	12	877	115	6,413	694	25	10,203	3,982	0	375	527
SG2	120	1,307	803	86,375	3,325	218	140,686	1,746	0	342	509
SG3	119	1,462	1,017	84,718	3,498	244	141,354	1,573	0	344	542
SG4	121	1,442	1,130	86,817	3,762	270	140,266	2,174	0	339	444
SG5	116	1,906	1,301	77,468	4,521	382	140,412	1,908	0	256	452
SG6	116	1,472	843	79,327	3,651	241	139,302	2,388	0	278	342
SG7	116	2,119	2,289	67,954	8,149	1,018	139,071	1,441	0	230	361
SG8	119	1,432	924	80,246	3,890	247	139,797	1,959	0	351	309
SG9	118	1,395	1,022	85,693	4,668	325	137,846	1,900	0	368	512
SG10	116	1,787	1,233	77,539	5,196	352	137,691	1,751	0	260	469

GUAYATAYOC											
sample	TDS	Ca	Mg	Na	K	Li	Cl	SO4	CO3	HCO3	B
GG3	48	2,084	292	20,000	8070	45	58,500	7,560	0	384	310
GQ0	86	1,382	134	32,400	21,000	125	252,800	13,000	0	286	450
GG4	81	1,270	123	31,700	20,870	117	245,090	13,500	0	276	321
CENTENARIO											
sample	TDS	Ca	Mg	Na	K	Li	Cl	SO4	CO3	HCO3	B
CE0	343	320	7,550	112,300	8,170	1,020	192,700	19,980	-	-	3,765
CE1	26	831	916	6,752	966	65	14,595	2,960	0	498	365
CE2	26	508	604	7,134	843	23	14,276	3,056	0	496	277
CE3	41	395	1,196	10,613	2,860	106	17,133	12,461	0	322	434
CE4	45	842	1,217	11,767	2,914	133	18,466	12,663	0	343	581
CE5	49	619	2,277	10,450	3,025	377	21,493	12,184	0	494	402
DIABLILLOS											
sample	TDS	Ca	Mg	Na	K	Li	Cl	SO4	CO3	HCO3	B
DI1	38	791	1,634	9,533	746	47	21,897	3,541	0	230	360
DI2	26	794	1,121	6,943	687	81	15,041	2,715	0	376	584
DI3	78	1,402	933	21,535	7,876	235	38,270	9,587	0	351	808
DI4	81	1,486	964	21,784	6,370	357	37,731	11,618	0	334	614
HOMBRE MUERTO											
sample	TDS	Ca	Mg	Na	K	Li	Cl	SO4	CO3	HCO3	B
MH0	341	1,000	268	121,900	9,340	914	194,800	11,100	-	-	1,455
HM1	31	792	916	8,197	2,984	114	18,766	1,017	0	133	377
HM2	33	410	678	8,871	4,310	85	19,490	1,216	0	204	538
HM3	194	1,162	1,114	64,927	6,430	966	137,910	1,284	0	62	1,323
HM4	205	592	833	72,484	4,022	674	139,409	1,312	0	321	515
HM5	196	874	1,915	62,400	5,660	1,013	125,313	934	0	105	1490
INCAHUASI											
sample	TDS	Ca	Mg	Na	K	Li	Cl	SO4	CO	HC	B

									3	O3	
IN1	48	1,284	5283	7,360	2,754	22	32,631	362	0	315	114
IN2	69	976	10,376	6,548	6,896	82	48,675	930	0	75	558
IN3	100	1,194	15,894	12,344	4,012	132	72,913	678	0	15	510
IN4	107	988	14,687	11,782	7,130	145	74,353	736	0	44	570
IN5	86	1,074	9828	10,491	7,732	96	61,345	855	0	276	427
PASTOS GRANDES (PUNA)											
sample	TDS	Ca	Mg	Na	K	Li	Cl	SO4	CO3	HCO3	B
PG0	333	740	2,980	118,200	4,730	440	178,700	26,080	-	-	2,220
PG1	154	766	3,785	50,220	919	[illegible]	97,053	968	0	822	702
PG2	227	745	2,431	80,732	652	510	161,390	970	0	896	784
PG3	157	512	4,479	50,673	5,506	410	102,850	970	0	980	300
PG4	158	580	5,646	49,772	3,590	305	101,060	943	0	955	455
PG5	158	498	5,611	41,464	5,914	857	91,505	14,903	0	865	812
POZUELOS											
sample	TDS	Ca	Mg	Na	K	Li	Cl	SO4	CO3	HCO3	B
PZ1	237	447	1,133	89,661	1,011	96	154,521	8,864	0	213	650
PZ2	291	558	1,854	107,772	2,976	207	176,283	9,060	0	278	1,366
PZ3	290	2,332	2,587	102,715	6,314	712	178,250	10,785	0	12	398
PZ4	239	604	1,816	115,975	4,044	260	198,970	2,974	0	0	1,655
PZ5	254	1,605	1,715	87,012	5,213	940	150,670	13,115	0	0	2,102
PZ6	295	1,610	2,099	102,152	4,728	835	190,956	9,685	0	0	202
PZ7	256	444	1,180	91,674	1,024	86	171,360	8,812	0	240	415
PZ8	205	672	741	76,591	816	75	122,034	9,005	0	266	396
RATONES											
sample	TDS	Ca	Mg	Na	K	Li	Cl	SO4	CO3	HCO3	B
RA1	28	1,213	135	9,780	852	88	17,260	2,731	0	647	312
RA2	83	1,540	323	30,533	3,205	260	54,457	5,125	0	415	433
RA3	72	1408	210	27,31	3,024	125	53,19	3,580	0	348	509

				2			2				
ANTOFALLA											
sample	TDS	Ca	Mg	Na	K	Li	Cl	SO4	CO3	HCO3	B
AN1	55	2,964	705	15,975	2,490	164	29,058	8,714	0	77	530
AN2	185	662	725	63,713	3,518	615	113,985	7,725	0	358	815
AN3	148	535	816	55,770	807	311	88,201	7,815	0	241	878
AN4	25	1,310	365	6,889	365	95	14,100	1,830	0	710	814
AN5	19	692	644	5,271	476	46	9,460	1,005	0	865	807
AN6	9	286	206	2,580	166	25	4,873	356	0	492	415
ARIZARO											
sample	TDS	Ca	Mg	Na	K	Li	Cl	SO4	CO3	HCO3	B
AR0	321	760	1,840	119,500	160	168	190,700	9,260	-	-	138
AR1	274	415	484	100,581	4,112	106	182,213	12,483	0	81	1,109
AR2	155	473	545	53,107	2,061	83	98,090	5,521	0	122	2,066
AR3	92	512	1,616	23,450	5,686	375	42,611	17,620	0	74	1,216
AR4	130	517	7,735	25,565	7,543	318	58,847	30,246	0	119	3,306
AR5	308	429	4,114	99,478	10,071	180	184,234	30,390	0	225	3,225
AR6	80	515	513	24,944	1,098	112	39,243	13,923	0	96	1,232
AR7	105	494	4,092	24,990	10,011	465	56,897	17,620	0	60	1,313
AR8	48	515	1,070	15,564	1,480	52	23,468	7,922	0	93	2,366
AR9	32	432	376	10,805	1,315	97	16,662	2,497	0	75	3,382
AR10	64	410	484	22,530	1,180	122	38,534	7,682	0	74	380
POCITOS											
sample	TDS	Ca	Mg	Na	K	Li	Cl	SO4	CO3	HCO3	B
PC0	327	600	1,290	123,100	3,400	97	190,600	7,440	-	-	708
PC1	32	1,235	246	9,584	421	27	18,020	2,690	0	74	70
PC2	34	1,443	285	9,667	105	30	17,859	6,240	0	56	85
PC3	278	795	1,225	102,597	610	101	182,235	9,050	0	0	208
PC4	299	815	1,384	110,862	1,197	86	190,750	4,300	0	0	194
PC5	38	1,54	260	11,44	1,488	46	18,34	6,955	0	37	88

		0		0			5				
PC6	41	412	568	12,544	1,670	65	23,950	5,272	0	37	170
PC7	36	645	633	10,380	1,771	68	16,055	7,925	0	0	162
PC8	29	408	596	10,301	1,612	53	15,252	3,897	0	15	60
PC9	30	944	578	10,298	1,644	22	18,095	2,102	0	22	63
PC10	45	365	135	12,863	1,702	68	20,333	9,970	0	13	63

RINCON

sample	TDS	Ca	Mg	Na	K	Li	Cl	SO4	CO3	HCO3	B
RI0	339	280	2,120	122,200	6,570	350	190,500	15,990	-	-	1,609
RI1	281	1,050	1,815	95,235	7,130	344	176,936	17,484	0	150	1,904
RI2	285	813	2,297	99,199	6,543	270	172,557	25,233	0	134	2,098
RI3	152	805	2,210	47,030	5,012	112	84,823	13,314	0	163	1,612
RI4	145	833	2,284	47,764	4,841	122	83,635	14,584	0	177	1,405
RI5	140	1,102	1,788	41,[illegible]40	6,974	360	73,814	15,415	0	210	1,812
RI6	141	910	2,044	38,945	6,530	268	74,722	16,112	0	147	2,041
RI7	152	930	1,83[illegible]	50,163	6,812	195	96,231	10,341	0	207	1,904
RI8	183	652	2,030	61,240	7,315	651	108,378	11,012	0	215	1,412
RI9	187	8[illegible]4	1,918	59,152	7,015	337	107,500	10,404	0	219	1,787
RI10	18[illegible]	630	2,016	60,488	4,916	150	102,334	10,482	0	112	1,470

RIO GRANDE

sample	TDS	Ca	Mg	Na	K	Li	Cl	SO4	CO3	HCO3	B
RG0	260	800	2,600	92,400	3,710	420	148,900	10,610	-	-	1,673
RG1	285	1,862	2,215	96,485	3,012	336	162,840	18,680	0	416	414
RG2	280	1,966	2,190	98,187	3,305	274	163,773	19,990	0	297	302
RG3	257	1,987	2,136	89,373	3,315	468	169,085	8,654	0	25	415
RG4	207	2,104	2,230	77,910	3,588	502	131,528	6,940	0	76	545
RG5	260	1,970	1,390	87,761	2,469	139	166,235	4,974	0	72	348
RG6	259	2,103	1,505	99,828	2,645	152	164,615	5,134	0	98	366

RG7	252	2,100	2,234	103,466	3,316	480	162,200	4,909	0	44	423
RG8	199	1,283	2,974	74,572	2,890	692	131,665	2,022	0	366	315
RG 9	234	2,330	2,212	78,288	3,325	475	150,755	3,080	0	381	442
RG10	226	2,049	2,084	75,342	3,191	443	147,765	2,315	0	337	404

- not reported

Table 3. Mean values for hydrochemical compositions of brines from Andean salt pans. Values correspond to averages computed on data presented in Table 2. n: number of samples. TDS in g L^{-1}, the remaining concentrations in mg L^{-1}.

N°	Salt pan	n	TDS	Ca	Mg	Na	K	Li	Cl	SO_4	CO_3	HCO_3	B
1	Surire	3	178	967	2,221	56,103	9,203	359	96,060	8,997	13	99	1,848
2	Coipasa	11	145	360	12,211	104,836	9,155	258	178,091	37,355	-	785	883
3	Uyuni	165	123	550	15,533	87,670	12,389	715	183,885	17,149	-	4	646
4	Empexa	1	239	259	8,480	67,200	3,400	213	120,000	34,100	-	430	702
5	Huasco	3	93	221	1,964	21,722	4,508	160	37,694	8,977	<1	20	779
6	Coposa	6	20	246	869	5,430	534	16	8,890	3,710	3	146	19
7	Michincha	5	<1	31	13	28	12	<1	18	-	<1	46	<1
8	Alconcha	1	1	150	2	97	13	<1	90	-	0	87	3
9	Carcote	4	234	7,039	4,151	70,567	7,268	217	61,812	3,038	5	169	224
10	Ascotan	10	29	280	786	8,497	899	47	13,581	3,885	14	593	374

11	Pastos Grandes (Altiplano)	1	321	3,100	3,480	101,000	14,200	1,640	194,000	2,460	-	-	3,041
12	Atacama	10	181	606	4,064	46,793	8,706	562	90,047	9,856	<1	273	482
13	El Tara	12	35	346	165	22,504	243	140	35,240	3,083	12	772	201
14	Aguas Calientes Norte	7	10	633	151	4,414	165	25	7,964	541	1	281	66
15	Pujsa	10	-	269	376	15,731	1,130	89	18,670	12,400	349	562	189
16	Loyoques o Quisquiro	5	94	11,454	1,960	53,698	409	280	141,913	1,615	8	599	480
17	Aguas Calientes Centro	5	17	1,225	946	6,060	394	15	12,460	1,740	0	339	7
18	El Laco	6	62	852	2,372	22,308	1,737	37	38,583	6,341	0	393	180
19	Aguas Calientes Sur	8	7	432	265	2,569	189	4	4,660	1,062	0	167	0
21	Imilac	4	5	321	32	8,948	49	19	2,374	801	4	59	4
22	Punta Negra	6	2	50	18	718	61	1	1,255	144	6	56	5
23	Aguas Calientes Sur Sur	10	4	202	131	1,668	163	5	2,718	1,014	7	108	19
24	Pajanoles	25	49	3,234	1,560	19,437	1,221	25	45,588	1,810	0	283	160
25	La Azufrera	2	287	441	34,400	42,317	10,773	61	121,157	65,834	0	36	532
26	Gorbea	5	58	288	26,810	47,060	3,925	316	114,070	72,389	0	0	2,319
27	Ignorados	2	11	495	576	490	490	2	927	6,895	0	0	24
28	Agua Amarga	6	75	16,652	2,411	34,783	1,429	60	92,098	1,095	0	121	311
29	Aguilar	3	113	51,667	6,600	60,667	2,600	367	203,334	461	0	917	739

30	La Isla	12	62	390	2,578	46,667	10,898	402	87,278	7,015	4	188	118
32	Las Parinas	6	46	300	1,185	36,317	1,114	130	59,607	4,501	0	326	148
34	Pedernales	4	1	143	47	735	53	3	1,285	342	2	112	10
38	Maricunga	3	19	517	252	5,988	485	36	11,309	172	0	167	26
39	Incahuasi	5	82	1,103	11,214	9,705	5,705	95	57,983	712	0	145	436
40	Antofalla-Botijuelas	6	73	1,075	577	25,033	1,304	209	43,280	4,574	0	457	710
41	Río Grande	11	247	1,869	2,161	88,510	3,161	298	154,487	7,937	0	211	513
42	Arizaro	11	147	497	2,082	47,320	4,156	188	84,682	14,106	0	102	1,794
43	Hombre Muerto	6	167	805	954	53,463	5,458	628	105,948	2,811	0	165	950
44	Diablillos	4	56	1,119	1,226	14,949	3,920	180	28,235	6,865	0	323	592
45	Ratones	3	61	1,387	223	22,542	2,360	158	41,636	3,812	0	470	418
46	Centenario	6	88	586	2,293	26,503	3,130	288	46,444	10,551	0	431	971
47	Pocitos-Quirón	11	108	837	655	38,512	1,420	60	64,681	5,986	0	25	170
48	Pozuelos	8	266	1,072	1,641	96,694	3,266	401	167,880	9,038	0	126	898
49	Pastos Grandes (Puna)	6	198	640	4,155	65,177	3,552	476	122,093	7,472	0	904	879
50	Rincón	11	199	823	2,032	65,696	6,333	287	115,585	14,579	0	173	1,732
51	Cauchari	5	119	600	1,746	83,886	4,757	860	130,867	12,306	0	442	2,158
52	Olaroz	10	154	516	2,002	98,846	6,224	1,014	180,798	10,077	0	344	2,533

53	Jama	10	32	527	228	20,424	1,469	82	32,306	6,633	0	309	983
54	Salinas Granes	10	107	1,520	1,068	73,255	4,135	332	126,663	2,082	0	314	447
55	Guayatayoc	3	72	1,579	183	28,033	16,647	96	185,463	11,353	0	315	360

Table 4. Summary of mean, maximum (*max*), and concentration ratios of Li^+ and Mg^{2+} in brines from Andean salt pans. The * values for the Atacama brines follow Moraga et al. (1974), Ide and Kunasz (1989), and Kunasz (2006). The * mean Li^+ concentration for Olaroz is from García et al. (2019). Remaining values and ratios correspond to data presented in Table 3.

No	salt pan	mean Li^+ (mg L^{-1})	mean Mg^{2+} (mg L^{-1})	*max* Li^+ (mg L^{-1})	*max* Mg^{2+} (mg L^{-1})	Mg:Li mean ratio	*max*:mean Li ratio
1	Surire	359	2,291	540	3,830	6	2
2	Coipasa	253	12,211	416	23,000	47	2
3	Uyuni	715	15,533	4,720	75,300	22	7
4	Empexa	213	8,480	213	8,480	40	1
5	Huasco	160	1,964	480	5,880	12	3
6	Coposa	16	869	90	4,930	56	6
7	Michincha	<1	13	<1	25	641	2
8	Alconcha	<1	2	<1	2	16	1
9	Carcote	217	4,151	339	6,850	19	2
10	Ascotan	47	786	245	5,125	17	5
11	Pastos Grandes (Altiplano)	1,640	3,480	1,640	3,480	2	1
12	Atacama	562 - 1,400*	4,064	1,570 - 6,400*	9,650 - 80,000*	7	3 - 5*
1	El Tara	140	165	420	440	1	3

Aguas Calientes Norte	25	151	130	820	6	5
Pujsa	89	376	400	3,762	4	5
Loyoques	286	1,960	425	2,855	7	1
Aguas Calientes Centro	15	946	45	7,981	63	3
El Laco	37	2,372	101	6,250	64	3
Aguas Calientes Sur	4	265	17	1,370	67	4
Imilac	19	32	73	66	2	4
Punta Negra	1	18	3	53	18	3
Aguas Calientes Sur Sur	5	131	35	1,311	25	7
Pajonales	25	1,560	62	5,200	63	3
La Azufrera	61	34,400	86	48,640	562	1
Gorbea	516	26,810	500	4,225	85	2
Ignorados	2	576	2	707	339	1
Aguas Amarga	60	2,411	157	39,500	40	3
Aguilar	367	6,600	375	6,900	18	1
La Isla	402	2,578	1,150	8,300	6	3
Las Parinas	130	1,185	400	3,600	9	3
Pedernales	3	47	3	58	15	1

Maricunga	36	252	92	680	7	3
Incahuasi	95	11,214	145	15,896	118	2
Antofalla-Botijuelas	209	577	615	816	3	3
Rio Grande	398	2,161	692	2,234	5	2
Arizaro	188	2,082	465	7,736	11	2
Hombre Muerto	628	954	1,013	1,915	2	2
Diablillos	180	1,226	[illegible]	1,884	7	2
Ratones	158	223	260	323	1	2
Centenario	288	[illegible]	1,020	7,550	8	4
Pocitos-Quirón	60	[illegible]	101	1,384	11	2
Pozuelos	[illegible]	1,641	940	2,587	4	2
Pastos Grandes (Puna)	[illegible]	4,155	857	5,647	9	2
Rincon	287	2,032	651	2,297	7	2
Cacuhari	860	1,746	1,740	2,104	2	2
Olaroz	1,014 - 841*	2,002	1,213	2,301	2	1
Jama	82	228	262	492	3	3
Salinas Grandes	332	1,068	1,018	2,289	3	3
Guayatayoc	96	183	125	183	2	1

Highlights

- Sizes of Andean salt pans are proportional to the extent of their endorheic basin.
- The equation *mean* Li ≈ ½ *max* Li is a tool for surveying of brine-type deposits.
- The greatest Li levels are expected to be found in largest and oldest salt pans.